

Extra-Natural Inflation (De)constructed

Kazuyuki Furuuchi, Noel Jonathan Jobu
and
Suvedha Suresh Naik

*Manipal Centre for Natural Sciences
Centre of Excellence
Manipal Academy of Higher Education
Dr. T.M.A. Pai Planetarium Building
Manipal 576 104, Karnataka, India*

Abstract

Extra-natural inflation is (de)constructed. Explicit models are compared with cosmological observations. The models successfully achieve trans-Planckian inflaton field excursions.

Contents

1	Introduction	1
2	Extra-natural inflation (de)constructed	3
3	Comparison of explicit models with CMB observations	7
3.1	Multi-natural inflation from (de)construction	7
3.2	Particle production during inflation	19
4	Summary and discussions	20
A	Discrete Fourier Transform	21
B	One-loop effective potential	23
C	Fitting Functions	30

1 Introduction

Dimensional (de)construction [1, 2] provides purely 4D QFT description of latticized extra dimensions. (De)construction of the gauge-Higgs unification model [3, 4, 5, 6, 7] has provided a new mechanism to protect the Higgs mass against quantum corrections [8]. Many mechanisms which were used to explain the lightness of the Higgs mass have also been used to explain the flatness of the potential of slow-roll inflation models. In the case of the gauge-Higgs unification model, extra-natural inflation [9, 10] employs the same mechanism in slow-roll inflation and provides a microscopic theory of natural inflation [11] from extra dimensions. Given the (de)construction of the gauge-Higgs unification model, it is natural to explore (de)construction of extra-natural inflation. However, already in the original work [9], it has been noticed that (de)construction of extra-natural inflation with one (de)constructed extra dimension does not lead to a successful model of slow-roll inflation. The obstacle was as follows: The basic natural inflation model is a large field inflation model which is required to have a trans-Planckian inflaton field excursion to explain observations of Cosmic Microwave Background (CMB) anisotropy. The trans-Planckian inflaton excursion requires $2\pi F \gg M_P$, where $2\pi F$ is the period of the inflaton potential and M_P is the reduced 4D Planck scale. However, in (de)construction models with one (de)constructed extra dimension, F is related to a symmetry breaking scale f in the model as $F = f/\sqrt{N}$, where N is the number of the lattice points in the (de)constructed dimension. For the model to be described without taking into account strong quantum gravity effects, $f \ll M_P$ is required, leading $F \ll M_P$. This poses an

obstacle for having the trans-Planckian inflation excursion. Thus nearly two decades after (de)construction was proposed, there has been no notable application of it in inflation model building. However, recently two ways to circumvent the above obstruction have been found [12]. One is to introduce a gauge-invariant Stueckelberg potential which gives rise to the dominant part of the inflaton potential. The gauge invariant Stueckelberg potential is not periodic under the shift of the inflaton, which originates from the extra-dimensional component of the gauge field.¹ Therefore, the inflaton field excursion is not restricted by the periodicity $2\pi F$. Another way to circumvent the obstruction is to increase the number of (de)constructed extra dimensions. It was shown in [12] that the period $2\pi F$ of the inflaton is related to the symmetry breaking scale f as $F = fN^{\frac{d}{2}-1}$, where d is the number of the (de)constructed extra dimensions and N is the number of the lattice points in each direction.² Therefore, for $d \geq 3$, the period $2\pi F$ of the inflaton potential can be much larger than the symmetry breaking scale f if N is sufficiently large, and this may enable the trans-Planckian inflaton excursion. In [12], the first way was the main focus, while the second way was briefly mentioned. In this article, we will study the second way in more detail. We construct explicit inflation models in which the zero-mode of a gauge field in one of the (de)constructed direction is an inflaton, and the field range of the inflaton is enhanced by (de)construction to enable the trans-Planckian excursion. Then we study the constraints on the parameters of the models from CMB observations.

The organization of this article is as follows: In Sec. 2 we present the theoretical framework of the (de)construction of extra-natural inflation. We start with a high energy theory with a product gauge group, and derive the low energy effective action which is appropriate below the energy scale of the gauge symmetry breaking to the diagonal subgroup. One of the (de)constructed extra dimensional components of the gauge field is to be identified with the inflaton. The one-loop effective potential for the inflaton is derived. The charged matter field contents determine the one-loop effective potential. In Sec. 3 we compare the models with explicit choice of the charged matter field contents with CMB observations. With charged matter fields having different charges, the (de)construction models provide microscopic theories of a version of natural inflation called multi-natural inflation [14], which can explain the latest CMB observations well. The observational constraints on the model parameters are derived. In a region of the model parameters, our (de)constructed models of extra-natural inflation successfully describe large-field inflation. We conclude with summary and discussions in Sec. 4. Some useful formulas and technical details are collected in the Appendices.

¹Since the periodicity of the action originates from the gauge invariance, it must be an exact symmetry. However, the gauge symmetry transformation involves the transformation of the Stueckelberg field. Thus the potential is not periodic if only the gauge field is shifted [13].

²Here, for simplicity, the number of the lattice points in all (de)constructed dimensions are chosen to be the same. In the main body, we will use an improved choice of parameters which makes the $d = 2$ case also worth examining.

2 Extra-natural inflation (de)constructed

The theoretical framework for (de)constructing extra-natural inflation have already been developed in [12], which studied (de)construction of a massive gauge theory. More detailed calculations and explanations are given there, and interested readers are encouraged to read the above reference together.

The (de)constructed extra dimensions we consider will be a d -dimensional periodic lattice (a lattice on a d -dimensional torus) with N_I ($I = 1, 2, \dots, d$) lattice points in the I -th direction. The model with such (de)constructed extra dimensions is described by the following 4D action:

$$\begin{aligned}
 S_{(4+d)} = \int d^4x \sum_{\vec{j}} \left\{ -\frac{1}{4} F_{\mu\nu(\vec{j})} F^{\mu\nu}_{(\vec{j})} + \sum_{I=1}^d \frac{f_I^2}{2} D_\mu U^I_{(\vec{j}, \vec{j} + \vec{e}_I)} D^\mu U^{I\dagger}_{(\vec{j}, \vec{j} + \vec{e}_I)} \right. \\
 \left. + \frac{1}{2} \beta_{IJ} g^2 f_I^2 f_J^2 \operatorname{Re} \left[U^I_{(\vec{j}, \vec{j} + \vec{e}_I)} U^J_{(\vec{j} + \vec{e}_I, \vec{j} + \vec{e}_I + \vec{e}_J)} U^{I\dagger}_{(\vec{j} + \vec{e}_J, \vec{j} + \vec{e}_I + \vec{e}_J)} U^{J\dagger}_{(\vec{j}, \vec{j} + \vec{e}_J)} \right] \right. \\
 \left. + \mathcal{L}_{matter} + \dots \right\}, \\
 (\mu = 0, 1, 2, 3; I = 1, 2, \dots, d; j_I = 0, 1, \dots, N_I - 1 \bmod N_I). \quad (2.1)
 \end{aligned}$$

Here, “...” represent higher dimensional operators which are irrelevant at low energy. The matter Lagrangian density \mathcal{L}_{matter} will be specified later. The I -th component of \vec{j} is denoted as j_I . The d -dimensional vector \vec{j} parametrizes the lattice points. \vec{e}_I is a vector whose J -th component is given by δ_{IJ} . The field $U^I_{(\vec{j}, \vec{j} + \vec{e}_I)}$ can be regarded as a parametrization of the Nambu-Goldstone boson from a global $U(1)$ symmetry breaking with the symmetry breaking scale f_I [1]. At the same time, in the language of lattice gauge theory, it is a link variable connecting the lattice points \vec{j} and $\vec{j} + \vec{e}_I$. This lattice (de)constructs effective extra dimensions from purely 4D QFT. The link variables can be parametrized as

$$U^I_{(\vec{j}, \vec{j} + \vec{e}_I)} = \exp \left[i \frac{A^I_{(\vec{j}, \vec{j} + \vec{e}_I)}}{f_I} \right]. \quad (2.2)$$

In the language of 4D QFT, the field $A^I_{(\vec{j}, \vec{j} + \vec{e}_I)}$ is analogous to the pion field, which is the approximate Nambu-Goldstone boson from the chiral symmetry breaking. At the same time, in the language of lattice gauge theory, the fields $A^I_{(\vec{j}, \vec{j} + \vec{e}_I)}$'s make up the gauge field in the (de)constructed directions.

The action (2.1) has the product $\prod_{\vec{j}} U(1)_{(\vec{j})}$ gauge symmetry. We also impose the symmetry under the discrete translation:

$$\vec{j} \rightarrow \vec{j} + \vec{e}_I \quad (I = 1, 2, \dots, d), \quad (2.3)$$

so that the gauge coupling g is the same for all $U(1)_{(\vec{j})}$. The gauge transformation generated by $g_{(\vec{j})}(x) = e^{ig\alpha_{(\vec{j})}(x)}$ are given as

$$A_{\mu(\vec{j})}(x) \rightarrow A_{\mu(\vec{j})}(x) - \partial_{\mu}\alpha_{(\vec{j})}(x), \quad (2.4)$$

$$U_{(\vec{j},\vec{j}+\vec{e}_I)}^I(x) \rightarrow g_{(\vec{j})}^{-1}(x)U_{(\vec{j},\vec{j}+\vec{e}_I)}^I(x)g_{(\vec{j}+\vec{e}_I)}(x). \quad (2.5)$$

The covariant derivative in (2.1) is defined as

$$D_{\mu}U_{(\vec{j},\vec{j}+\vec{e}_I)}^I = \partial_{\mu}U_{(\vec{j},\vec{j}+\vec{e}_I)}^I - igA_{\mu(\vec{j})}U_{(\vec{j},\vec{j}+\vec{e}_I)}^I + igU_{(\vec{j},\vec{j}+\vec{e}_I)}^IA_{\mu(\vec{j}+\vec{e}_I)}. \quad (2.6)$$

Following the terminology in lattice gauge theory, we may define the lattice spacing in the I -th direction as

$$a_I := \frac{1}{gf_I} \quad (I = 1, 2, \dots, d). \quad (2.7)$$

We may also define the compactification radius of the I -th direction as

$$2\pi L_I := N_I a_I = \frac{N_I}{gf_I} \quad (I = 1, 2, \dots, d). \quad (2.8)$$

The mass-square matrix of the gauge fields in the vacuum $U_{(\vec{j},\vec{j}+\vec{e}_I)}^I = 1$ can be read off from the action (2.1):

$$M_g^2 := \sum_{I=1}^d M_{gI}^2 := g^2 \sum_{I=1}^d f_I^2 \mathbb{1}_{N_1} \otimes \dots \otimes \mathbb{1}_{N_{I-1}} \otimes K_{N_I} \otimes \mathbb{1}_{N_{I+1}} \otimes \dots \otimes \mathbb{1}_{N_d}, \quad (2.9)$$

where $\mathbb{1}_{N_J}$ denotes the $N_J \times N_J$ identity matrix and K_{N_I} is the $N_I \times N_I$ matrix given as

$$K_{N_I} := \begin{pmatrix} 2 & -1 & 0 & 0 & \dots & -1 \\ -1 & 2 & -1 & 0 & \dots & 0 \\ 0 & -1 & 2 & -1 & \dots & 0 \\ \vdots & & & \ddots & & \vdots \\ 0 & \dots & & & 2 & -1 \\ -1 & \dots & & & -1 & 2 \end{pmatrix}. \quad (2.10)$$

The mass-square eigenvalues can be obtained using the Discrete Fourier Transform (DFT):

$$A_{(\vec{j},\vec{j}+\vec{e}_I)}^I = \frac{1}{\prod_{J=1}^d N_J^{1/2}} \sum_{\vec{n}} \tilde{A}_{(\vec{n})}^I e^{i \sum_{K=1}^d \frac{2\pi n_K j_K}{N_K}}. \quad (2.11)$$

Our convention for DFT is given in Appendix A. In (2.11), the sum over \vec{n} follows our convention (A.1) or (A.2) for each component n_I . The mass-square eigenvalues $M_{gI}^2(\vec{n})$ can be parametrized by the discrete Fourier mode \vec{n} and given as

$$M_{gI}^2(\vec{n}) = 4g^2 f_I^2 \sin^2 \left(\frac{\pi n_I}{N_I} \right) = \left(\frac{2}{a_I} \right)^2 \sin^2 \left(\frac{\pi n_I}{N_I} \right). \quad (2.12)$$

The product gauge group $\prod_{\vec{j}} U(1)_{(\vec{j})}$ is spontaneously broken to the diagonal $U(1)$ which corresponds to the zero-mode $\vec{n} = \vec{0}$. From (2.12) and using (2.8), we observe that in large N_I limit the mass spectrum approaches the Kaluza-Klein (KK) mass spectrum of the ordinary d -dimensional torus with the radius of the I -th direction being L_I . We will use the same terminology in continuous extra dimensions for a corresponding quantity in (de)constructed extra dimensions when the correspondence is obvious (e.g. KK scale).

The second line in (2.1) corresponds to the Wilson plaquette action in the language of lattice gauge theory. A natural magnitude of the real coupling constant β_{IJ} is of order one, as can be estimated from the dimensional analysis with symmetry considerations [8, 15]. With β_{IJ} of order one, the extra-dimensional components of the gauge field acquire masses of the order of the KK scale in the vacuum except for the zero-modes, like the space-time components of the gauge field (see (2.12)).

The matter Lagrangian density \mathcal{L}_{matter} in (2.1) is a sum of Lagrangian densities of charged matter fields. For simplicity, we consider scalar fields $\chi_{(\vec{j})}^q$ which has a charge q under the $U(1)_{(\vec{j})}$ gauge group. The charge q of the scalar field $\chi_{\vec{j}}^q$ is the same for all \vec{j} to respect the symmetry under the discrete translation (2.3), like the gauge coupling g . The $U(1)_{(\vec{j})}$ gauge group is compact and thus the charges are quantized. We normalize the gauge coupling g so that all charges in the model are integers. The Lagrangian density of the charged scalar field with charge q is given by

$$\begin{aligned} \mathcal{L}_q = & D_\mu \chi_{(\vec{j})}^{q\dagger} D^\mu \chi_{(\vec{j})}^q - m^2 \chi_{(\vec{j})}^{q\dagger} \chi_{(\vec{j})}^q \\ & - \sum_{I=1}^d \left[\gamma_I^q f_I^2 \left(\left(U_{(\vec{j}, \vec{j} + \vec{e}_I)}^I \right)^q \chi_{(\vec{j} + \vec{e}_I)}^q - \chi_{(\vec{j})}^q \right)^\dagger \left(\left(U_{(\vec{j}, \vec{j} + \vec{e}_I)}^I \right)^q \chi_{(\vec{j} + \vec{e}_I)}^q - \chi_{(\vec{j})}^q \right) \right], \end{aligned} \quad (2.13)$$

where the covariant derivative for the charged matter with charge q is given as

$$D_\mu \chi_{(\vec{j})}^q = \partial_\mu \chi_{(\vec{j})}^q - igq A_{\mu(\vec{j})} \chi_{(\vec{j})}^q. \quad (2.14)$$

We will eventually be interested in the zero-mode of the first component of the extra-dimensional components of the gauge field, which will play the role of the inflaton:

$$\phi := \tilde{A}_{(\vec{0})}^1 = \frac{1}{\prod_{I=1}^d N_I^{1/2}} \sum_{\vec{j}} A_{(\vec{j}, \vec{j} + \vec{e}_1)}^1. \quad (2.15)$$

As shown in Appendix B (see (B.24)), each massless³ charged scalar field contributes to the effective potential of the zero-mode ϕ at one-loop level as

$$V^q(\phi) = -\Lambda^4 \cos \left[\frac{q\phi}{F} \right], \quad (2.16)$$

³As explained in Appendix B, when estimating the one-loop effective potential, we will treat fields whose mass is far below the KK energy scale as massless, while we will drop the contributions from fields whose mass is above the KK energy scale.

where

$$\begin{aligned}\Lambda^4 &= \frac{1}{2(4\pi)^2} \frac{2^d}{\pi^{d/2}} \Gamma\left(2 + \frac{d}{2}\right) (2\pi L_1)(2\pi L)^{d-1} \left(\frac{4}{(2\pi L_1)^2}\right)^{2+\frac{d}{2}} \\ &= \frac{1}{2(4\pi)^2} \frac{2^d}{\pi^{d/2}} \Gamma\left(2 + \frac{d}{2}\right) N_1 N^{d-1} \left(\frac{2}{N_1}\right)^{4+d} (gf)^4,\end{aligned}\quad (2.17)$$

and

$$F = \frac{N^{\frac{d-1}{2}} f}{N_1^{\frac{1}{2}}}.\quad (2.18)$$

In the above, we have set

$$f_I = f \quad (\text{for all } I),\quad (2.19)$$

$$N_I = N \quad (\text{for all } I \neq 1),\quad (2.20)$$

$$N \gg N_1.\quad (2.21)$$

From (2.8), the simplifying assumptions (2.19) and (2.20) make all L_I except for $I = 1$ equal, which we call L : $L_I = L$ for all $I \neq 1$. Together with the simplifying assumptions (2.19) and (2.20), the condition (2.21) can be used to make the low energy effective potential such that $\phi = \tilde{A}_{(\bar{0})}^1$ direction satisfies the slow-roll condition while $\tilde{A}_{(\bar{0})}^I$ directions ($I \neq 1$) do not. Then the model is described as a single-field inflation.

The low energy effective action which is appropriate below the KK-energy scale $1/L$ is given as

$$\begin{aligned}S_4 &= \int d^4x \left[\frac{1}{2} \partial_\mu \phi \partial^\mu \phi - V(\phi) \right. \\ &\quad \left. + \sum_{\text{charged matter}} \sum_{n_1} \left\{ D_\mu \tilde{\chi}_{(n_1)}^{q\dagger} D^\mu \tilde{\chi}_{(n_1)}^q - \tilde{\chi}_{(n_1)}^{q\dagger} M_{n_1}^2(q, \phi) \tilde{\chi}_{(n_1)}^q \right\} \right].\end{aligned}\quad (2.22)$$

Here, the inflaton potential is given as a sum of the contributions (2.16) from massless charged scalar fields:

$$V(\phi) = C' + \sum_q M_q V^q(\phi),\quad (2.23)$$

where M_q is the number of the massless scalar fields with charge q and C' is the constant.

In the covariant derivative of the charged scalar in the low energy effective action (2.22), only the zero-mode of the gauge field $A_{\mu(\bar{j})}$ appears:

$$D_\mu \tilde{\chi}_{(n_1)}^q = \partial_\mu \tilde{\chi}_{(n_1)}^q - ig_4 q \tilde{A}_{\mu(\bar{0})} \tilde{\chi}_{(n_1)}^q,\quad (2.24)$$

where

$$g_4 := \frac{g}{N_1^{\frac{1}{2}} N^{\frac{d-1}{2}}},\quad (2.25)$$

is the effective gauge coupling for the unbroken diagonal $U(1)$ gauge group. The field $\tilde{\chi}_{(n_1)}^q$ is the zero-mode in the $I \neq 1$ directions, i.e. the discrete Fourier mode $\tilde{\chi}_{(\vec{n})}^q$ with $n_I = 0$ for $I \neq 1$. However, the mass of the field $\tilde{\chi}_{(n_1)}^q$ depends on the expectation value of the inflaton:

$$M_{n_1}^2(q, \phi) = m^2 + 4\gamma_1^q f^2 \sin^2 \left(\frac{q\phi + 2\pi n_1 F}{2FN_1} \right)^2. \quad (2.26)$$

As can be seen from (2.26), which mode number n_1 gives the lightest mode depends on the expectation value of the inflaton field. Therefore, we kept all the discrete Fourier modes labeled by n_1 . The inflaton dependent mass (2.26) can have interesting consequences in inflation [13, 12], which we examine in Sec. 3.2.

3 Comparison of explicit models with CMB observations

3.1 Multi-natural inflation from (de)construction

The simplest natural inflation model [11] is described by a single sinusoidal inflaton potential:

$$V(\phi) = \frac{V_0}{2} \left(1 - \cos \frac{\phi}{F} \right). \quad (3.1)$$

The single sinusoidal inflaton potential is not favored by the latest CMB anisotropy data [16]. However, simple modifications to the single sinusoidal potential may improve the fit to the observational data. Here, we choose multi-natural inflation model [14] as such a simple modification with an improved fit to the observational data. The inflaton potential in this model is given by two sinusoidal potentials with different periodicities:

$$V(\phi) = C' - \Lambda^4 \left[\cos \left(\frac{\phi}{F} \right) + B \cos \left(\frac{\phi}{AF} + \theta \right) \right], \quad (3.2)$$

where C' , Λ' , A , B and θ are constant parameters. The (de)construction of extra-natural inflation we developed in the previous section provides a microscopic theory of the multi-natural inflation model. In terms of the (de)construction model parameters, the potential (3.2) is parametrized as (see (2.23))

$$V(\phi) = M_1 \Lambda^4 \left[C - \cos \left(\frac{\phi}{F} \right) - B_q \cos \left(\frac{q\phi}{F} + \theta \right) \right]. \quad (3.3)$$

Comparing (3.2) and (3.3), we read off the relation between the parameters of multi-natural inflation and those in the microscopic (de)construction model: $\Lambda^4 = M_1 \Lambda^4$,

$A = 1/q$, $B = B_q$ and $C' = M_1 \Lambda^4 C$. In the (de)construction model, M_1 is identified with the number of the massless scalar fields with charge one, and B_q is given by

$$B_q := \frac{M_q}{M_1}, \quad (3.4)$$

where M_q is the number of the massless scalar fields with charge q , see (2.23). Λ is given by the (de)construction model parameters as in (2.17), while F is given as in (2.18). We will adjust the constant C so that the value of the potential at its minimum is zero. This fine-tuning is the usual cosmological constant problem which we will not address in this article.

While it would be possible to construct a microscopic (de)construction model which gives rise to non-zero θ in (3.3), such a model would need an additional mechanism to explain it.⁴ For simplicity, in this article we only consider models in which θ is zero. Setting $\theta = 0$ fixes the constant C from the requirement that the value of the potential at its minimum is zero:

$$C = (B_q + 1), \quad (3.5)$$

so that

$$V(\phi) = M_1 \Lambda^4 \left[\left(1 - \cos \left(\frac{\phi}{F} \right) \right) + B_q \left(1 - \cos \left(\frac{q\phi}{F} \right) \right) \right]. \quad (3.6)$$

From the inflaton potential (3.6), the slow-roll parameters are obtained as

$$\epsilon(\phi) = \frac{1}{2} \left(\frac{V'}{V} \right)^2 = \frac{1}{2F^2} \left(\frac{\sin \left(\frac{\phi}{F} \right) + B_q q \sin \left(\frac{q\phi}{F} \right)}{\left(1 - \cos \left(\frac{\phi}{F} \right) \right) + B_q \left(1 - \cos \left(\frac{q\phi}{F} \right) \right)} \right)^2, \quad (3.7)$$

$$\eta(\phi) = \frac{V''}{V} = - \frac{\cos \left(\frac{\phi}{F} \right) + B_q q^2 \cos \left(\frac{q\phi}{F} \right)}{F^2 \left(\left(1 - \cos \left(\frac{\phi}{F} \right) \right) + B_q \left(1 - \cos \left(\frac{q\phi}{F} \right) \right) \right)}. \quad (3.8)$$

Here and below, we work in the Planck units $M_P = 1$. We will use the subscript *end* to indicate that the value is at the time when inflation ends. More explicitly, we define the end of inflation as the time when the slow-roll condition breaks down:

$$\epsilon(\phi_{end}) = 1. \quad (3.9)$$

When $|q\phi_{end}| \ll F$, the Taylor expansion of $\epsilon(\phi_{end})$ gives

$$\phi_{end} \simeq \sqrt{2} \simeq 1.4. \quad (3.10)$$

⁴For example, non-zero θ can arise from an expectation value of an additional gauge field in the (de)constructed extra dimensions coupled to the charged scalar fields. In order for the model to have a non-zero value of θ , the model should be such that the corresponding gauge field has desired expectation value.

In the examples we will study, F is large enough to justify the approximation $\phi_{end} = 1.4$. Hence we will use this value for ϕ_{end} below.

The number of e-folds in slow-roll inflation is given by

$$\mathcal{N}_* = \int_{\phi_{end}}^{\phi_*} d\phi \left(\frac{V}{V'} \right). \quad (3.11)$$

Here and below, we use the subscript $*$ to indicate that it is the value when the pivot scale exited the horizon. Following the Planck 2018 results [16], we chose the pivot scale to be 0.002 Mpc^{-1} . The inflaton field value ϕ_* when the pivot scale exited the horizon is determined by setting the number of e-folds \mathcal{N}_* in (3.11).

The scalar power spectral index n_s and tensor-to-scalar ratio r are given by

$$n_s = 1 - 6\epsilon_* + 2\eta_*, \quad (3.12)$$

$$r = 16\epsilon_*. \quad (3.13)$$

In Fig. 1, we plot the predicted values of n_s and r for different choices of B_q and q , for $\mathcal{N}_* = 50$ and $\mathcal{N}_* = 60$, for a range of values of F . The predicted values of n_s and r are compared with the Planck 2018 results [16]. From Fig. 1, we observe that the predicted values of (n_s, r) enter observationally favored region for a range of values of F .

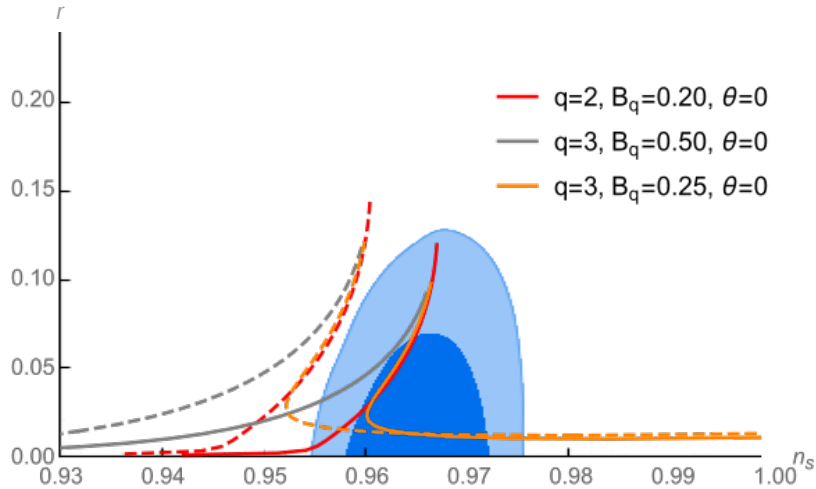


Figure 1: Predicted values of (n_s, r) of multi-natural inflation models for three sets of q and B_q values. The dashed and solid lines correspond to $\mathcal{N}_* = 50$ and $\mathcal{N}_* = 60$, respectively. These values are compared with the Planck 2018 68% and 95% confidence level regions of (n_s, r) ($TT, TE, EE + lowE + lensing$) [16].

The scalar power spectrum P_s from slow-roll inflation is given by

$$P_s = \frac{H^2(\phi_*)}{8\pi^2\epsilon_*} = \frac{V(\phi_*)}{24\pi^2\epsilon_*} = 2.2 \times 10^{-9}, \quad (3.14)$$

where H is the Hubble parameter and we have used the slow-roll approximation $3H^2(\phi) = V(\phi)$.

In the following, we study the observational constraints on models with explicit choices of q , B_q and M_1 . We first find the range of F allowed by the Planck 2018 results for a given model. Then from the constraint on the parameter F , we derive the constraints on the number of the lattice points N and N_1 for a given set of parameters. We will also examine independent constraints coming from the requirement that the model should be described by the low energy action (2.22) during inflation.

The model $q = 2$, $B_q = 0.2$, $M_1 = 5$ with $\mathcal{N}_* = 60$

We first study the model $q = 2$, $B_q = 0.2$, $M_1 = 5$ with $\mathcal{N}_* = 60$, which has a good overlap with the observationally allowed region in the n_s - r plane Fig. 1 for a range of parameters.

On the left in Fig. 2, the spectral index n_s is plotted for a range of F . The horizontal lines correspond to the upper and the lower bounds on n_s from the Planck 2018 results [16] with 68% confidence level (*Planck TT,TE,EE+lowE+lensing*):

$$n_s = 0.9649 \pm 0.0042. \quad (3.15)$$

On the right in Fig. 2, the tensor-to-scalar ratio r is plotted for a range of F . The horizontal line corresponds to the upper bound given in the Planck 2018 results [16] with 95% confidence level (*Planck TT+lowE+lensing*):

$$r < 0.10. \quad (3.16)$$

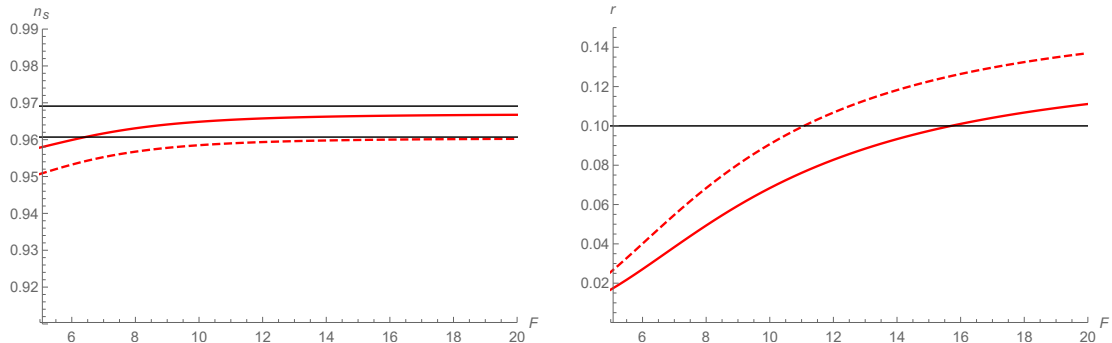


Figure 2: The plot of the power spectral index n_s (left) and the plot of the tensor-to-scalar ratio r (right) for a range of parameter F for the model $q = 2$, $B_q = 0.20$, $M_1 = 5$ with $\mathcal{N}_* = 50$ (red dashed line), $\mathcal{N}_* = 60$ (red bold line). The horizontal lines in the left plot show the lower and the upper bounds on n_s with 68% confidence level, and the horizontal line in the right plot shows the upper bound on r with 95% confidence level from the Planck 2018 results [16].

From the F - n_s plot on the left of Fig. 2, we find the lower bound of F for the number of e-folds $\mathcal{N}_* = 60$ as

$$F_{l.b.} = 6.4. \quad (3.17)$$

From the F - r plot, we find the upper bound of F for the number of e-folds $\mathcal{N}_* = 60$:

$$F_{u.b.} = 16. \quad (3.18)$$

The lower and the upper bound on F , (3.17) and (3.18), constrain the range of the number of the lattice points N and N_1 . To see this, we first substitute (3.6) and (3.7) in (3.14) to obtain

$$P_s = \frac{M_1 \Lambda^4 F^2 \left(\left(1 - \cos\left(\frac{\phi_*}{F}\right)\right) + B_q \left(1 - \cos\left(\frac{q\phi_*}{F}\right)\right) \right)^3}{12\pi^2 \left(\sin\left(\frac{\phi_*}{F}\right) + B_q q \sin\left(\frac{q\phi_*}{F}\right) \right)^2}. \quad (3.19)$$

For generic values of parameters, we cannot analytically perform integration in (3.11) to have explicit functional form of \mathcal{N}_* as a function of ϕ_* . However, notice that from (3.11) and (3.6), once q , B_q and \mathcal{N}_* are given, ϕ_* only depends on the parameter F . Consequently, from (3.19), $P_s/M_1\Lambda^4$ only depends on F . Let us denote this function of F as $\Phi[F]$:

$$\Phi[F] := \frac{P_s|_{q=2, B_q=0.2, \mathcal{N}_*=60}[F]}{M_1 \Lambda^4}. \quad (3.20)$$

In Fig. 3 we plot $\Phi[F]$ obtained by numerically solving (3.11) to obtain ϕ_* , and putting the obtained value of ϕ_* into (3.19), for a range of values of F .

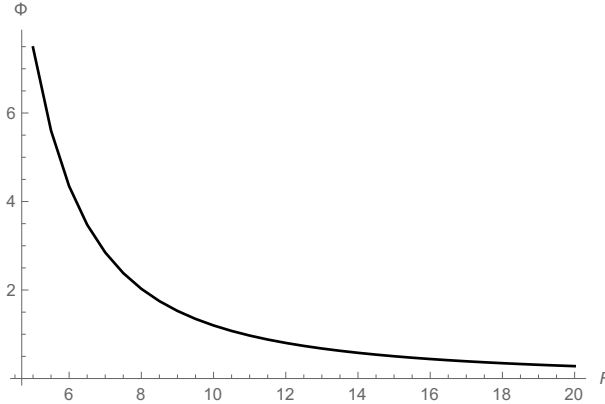


Figure 3: The plot of $\Phi[F]$ given in (3.20) for a range of the parameter F for the model $q = 2$, $B_q = 0.2$, $M_1 = 5$ with $\mathcal{N}_* = 60$.

Since Fig. 3 is numerically evaluated at each point in F , it may not be easy for the readers to read off the value of $\Phi[F]$ for a desired value of F . Therefore, in Appendix C, we provide a fitting function $\Phi_{fit}[F]$ which reproduces $\Phi[F]$ with around 1% level error or less for the range of F of interest.

The power spectrum P_s is fixed by the COBE normalization (3.14):

$$P_s = M_1 \Lambda^4 \Phi[F] = 2.2 \times 10^{-9}. \quad (3.21)$$

On the other hand, we can write Λ in terms of the (de)construction model parameters as in (2.17):

$$\Lambda^4 = \frac{1}{2(4\pi)^2} \frac{2^d}{\pi^{d/2}} \Gamma\left(2 + \frac{d}{2}\right) N_1 N^{d-1} \left(\frac{2}{N_1}\right)^{4+d} (gf)^4. \quad (3.22)$$

Substituting (3.22) into (3.21) and also using (2.18) to write N_1 in terms of f , F and N , we obtain N for a given set of parameters F , g , f , M_1 and the number of extra dimensions d :

$$N = \left(\frac{M_1 \Phi[F]}{2.2 \times 10^{-9}} \frac{2^{3+2d} \Gamma\left(2 + \frac{d}{2}\right)}{(4\pi)^2 \pi^{d/2}} \left(\frac{f^2}{F^2}\right)^{-(3+d)} (gf)^4 \right)^{\frac{1}{(d-1)(d+2)}}. \quad (3.23)$$

From the lower and the upper bound on F (3.17) and (3.18), we obtain constraints on N , and then through (2.18) constraints on N_1 . The constraints on N and N_1 for the model $q = 2$, $B_q = 0.2$, $M_1 = 5$ with $\mathcal{N}_* = 60$, $g = 1.0$, $f = 1.0 \times 10^{-2}$ are summarized in Table. 1.

d	Constraints on N	Constraints on N_1
2	$2.6 \times 10^7 \leq N \leq 1.5 \times 10^8$	$60 \leq N_1 \leq 65$
3	$3.9 \times 10^3 \leq N \leq 9.4 \times 10^3$	$35 \leq N_1 \leq 37$
4	$2.2 \times 10^2 \leq N \leq 4.0 \times 10^2$	$24 \leq N_1 \leq 25$
5	$53 \leq N \leq 83$	$19 \leq N_1 \leq 20$
6	$23 \leq N \leq 33$	$N_1 = 16$

Table 1: The constraints on N and N_1 derived from the lower and the upper bound on F , (3.17) and (3.18), for the model $q = 2$, $B_q = 0.2$, $M_1 = 5$ with $\mathcal{N}_* = 60$, $g = 1.0$, $f = 1.0 \times 10^{-2}$.

We observe that for $d \geq 5$, our assumption $N \gg N_1$ (2.21) may not hold well. In this case, the zero-modes of the extra-dimensional components of the gauge field in other directions are not too heavier than the inflaton, and the model may not be described as a single-field inflation. Actually, the condition that the model is described as a single-field inflation, or more explicitly the condition that the low energy effective potential in the direction of the zero-mode of the I -th component ($I \neq 1$) of the gauge field does not satisfy the slow-roll condition, can be stated a little bit more precise than (2.21). The periodicity $2\pi F'$ of the zero-mode in I -th direction ($I \neq 1$) is obtained as (see Appendix B eq.(B.12))

$$F' = \frac{N_1^{\frac{1}{2}} N^{\frac{d-1}{2}} f}{N} = \frac{N_1}{N} F. \quad (3.24)$$

The slow-roll parameters in the I -th direction ($I \neq 1$) is of the order of $1/F'^2$. Thus the condition that the I -th direction ($I \neq 1$) does not satisfy the slow-roll condition is

$$\frac{1}{F'^2} \gtrsim 1 \Rightarrow \frac{N}{N_1} \gtrsim F. \quad (3.25)$$

Indeed, the condition (3.25) does not hold for the cases $d = 5$ and $d = 6$. In the case $d = 4$, the left hand side and the right hand side of the inequality in (3.25) are of the same order and we may better have a closer look. In Fig. 4, N/N_1 and F are plotted for the range of F of interest. We observe that two lines in the plot intersect at $F = 17$, which is beyond $F_{u.b.}$ (3.18). Therefore, the condition (3.25) does not give a new constraint to this model. Also notice that the inequality in (3.25) allows the both sides to be around the same. Thus the region $F > 17$ should not be excluded immediately by (3.25). In fact, we observe from Fig. 4 that the both sides of (3.25) are around the same throughout the range of F of interest.

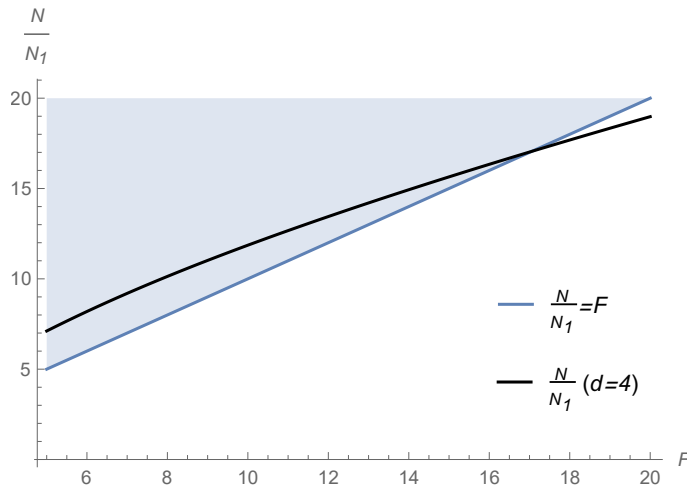


Figure 4: The plot of N/N_1 and the constraint on it that the model to be described as a single-field inflation model (3.25) for the range of F of interest.

We should also require the energy scale during inflation to be lower than the KK energy scale:

$$H \ll \frac{1}{L} = \frac{gf}{N}. \quad (3.26)$$

This condition is required for the low energy effective action (2.22) to be valid during inflation. In slow-roll inflation in which the inflaton rolls down the potential as time elapses, the Hubble parameter at the pivot scale $H_* := H(\phi_*)$ is close to the maximum value during the observable inflation. Therefore, we choose H_* as the representative value of H in (3.26). The value of H_* is obtained from (3.14). For fixed q , B_q and \mathcal{N}_* which we chose to be $q = 2$, $B_q = 0.2$ and $\mathcal{N}_* = 60$, H_* is a function only on the parameter F . The

numerically evaluated values of H_* are plotted for the range of F of interest in Fig. 5. Like we did for $\Phi[F]$, we also provide a fitting function for the square of the Hubble parameter in Appendix C. From Fig. 5 we observe that H_* is of the order of 10^{-5} . Putting $g \sim 1$ and $f \sim 10^{-2}$, (3.26) gives $N \ll 10^3$. Comparing this constraint with Table. 1, the cases $d \leq 3$ are excluded for these values of parameters g and f , while the $d \geq 5$ cases are safely in the allowed region. In the case $d = 4$, the allowed values of N in Table. 1 are comparable with the boundary of the constraint (3.26) in the range of F of interest, so we should have a closer look.

In Fig. 6, we plotted N for the case $d = 4$ and the constraint from (3.26). We observe that the region $F > 12$ is excluded by the constraint (3.26) for the case $d = 4$, and as a consequence N is restricted as $N \leq 3.3 \times 10^2$.

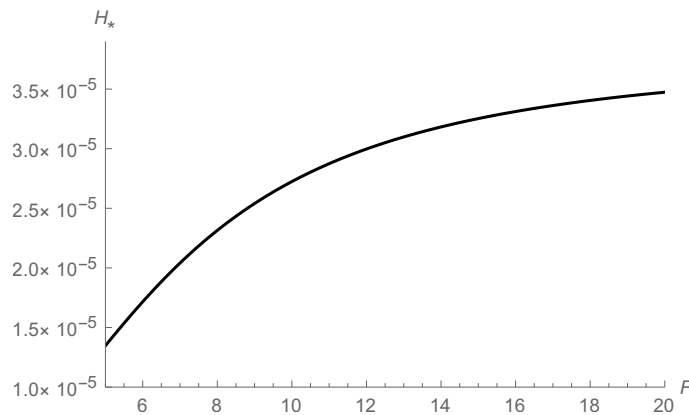


Figure 5: The plot of the Hubble parameter at the pivot scale for the range of F of interest $F_{l.b.} = 6.4 \leq F \leq F_{u.b.} = 16$.

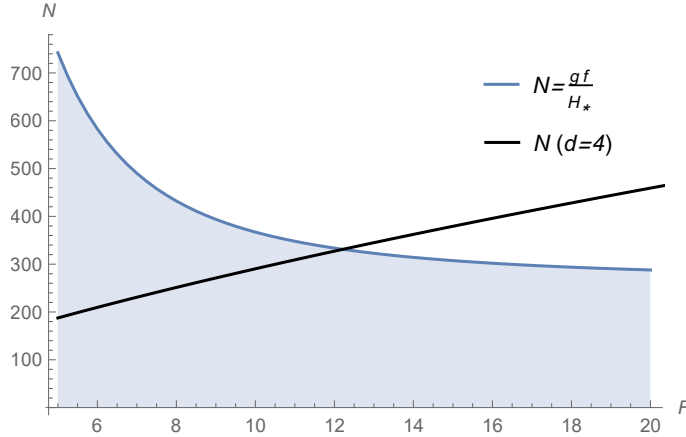


Figure 6: The constraint on N placed by (3.26) for the range of F of interest $F_{l.b.} = 6.4 \leq F \leq F_{u.b.} = 16$ for the model $q = 2$, $B_q = 0.2$, $M_1 = 5$ with $\mathcal{N}_* = 60$. The parameters g and f are fixed as $g = 1.0$ and $f = 1.0 \times 10^{-2}$ here. N for the case $d = 4$ in the same model with the same values of the parameters is plotted to be compared with the constraint.

To summarize the results of this model with the parameter values $\mathcal{N}_* = 60$, $g = 1.0$ and $f = 1.0 \times 10^{-2}$, the cases $d \leq 3$ are excluded by the condition (3.26), while in the cases $d \geq 5$ the condition (3.25) is not satisfied. In the case $d = 4$, we obtain $F \geq 6.4$ (which corresponds to $N \geq 2.2 \times 10^2$ and $N_1 = 25$) from the lower bound on n_s as in (3.17), and we obtain $F \leq 12$ (which corresponds to $N \leq 3.3 \times 10^2$ and $N_1 = 25$) from (3.26). Notice that in this range of the parameter F , the predicted tensor-to-scalar ratio r is above 0.01, as seen in Fig. 2. Via the Lyth bound [17], this means that the model belongs to large-field inflation models which enjoy the trans-Planckian inflaton field excursion.

The model $q = 3$, $B_q = 0.25$, $M_1 = 4$ with $\mathcal{N}_* = 60$

Next we study the model $q = 3$, $B_q = 0.25$, $M_1 = 4$ with $\mathcal{N}_* = 60$. Since the methodology is the same as in the previous model, we skip the explanations and only quote the results.

From the F - n_s plot on the left of Fig. 7, we find the lower bound of F from the upper bound on n_s :

$$F_{l.b.} = 6.9. \quad (3.27)$$

Here, although in the plot of n_s in Fig. 7, the model prediction slightly comes below the observational lower bound with 68% confidence level in the region around $F = 9 \sim 10$, we did not exclude this region as the differences from the lower bound are tiny.

From the F - r plot on the right, we find the upper bound of F :

$$F_{u.b.} = 26. \quad (3.28)$$

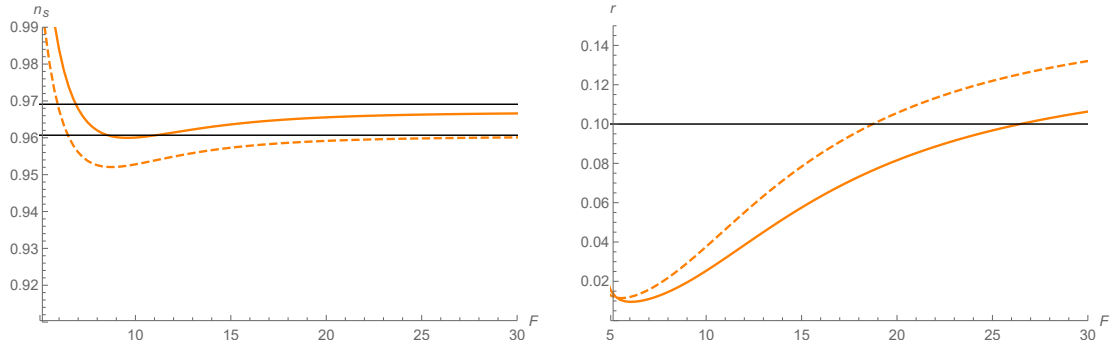


Figure 7: The plot of the power spectral index n_s (left) and the plot of the tensor-to-scalar ratio r (right) for a range of the parameter F for the model $q = 3$, $B_q = 0.25$, $M_1 = 4$ with $\mathcal{N}_* = 50$ (orange dashed line), $\mathcal{N}_* = 60$ (orange bold line). The horizontal lines in the left plot show the lower and the upper bounds on n_s with 68% confidence level, and the horizontal line in the right plot shows the upper bound on r with 95% confidence level from the Planck 2018 results [16].

With a bit of abuse of notation, we define the function $\Phi[F]$ in the same way as in (3.20) but for the current model:

$$\Phi[F] := \frac{P_s|_{q=3, B_q=0.25, \mathcal{N}_*=60}[F]}{M_1 \Lambda^4}. \quad (3.29)$$

The numerically evaluated values of $\Phi[F]$ for a range of values of F are plotted in Fig. 8. We also provide a fitting function $\Phi_{fit}[F]$ in Appendix C.

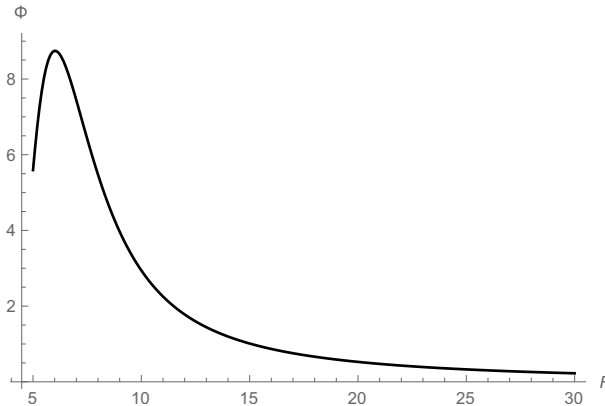


Figure 8: The plot of $\Phi[F]$ given in (3.29) for a range of F for the model $q = 3$, $B_q = 0.25$, $M_1 = 4$ with $\mathcal{N}_* = 60$.

Using (3.23), from the lower and the upper bound on F , (3.27) and (3.28), we obtain constraints on N , and then through (2.18) constraints on N_1 . The constraints on N and

N_1 for the model $q = 3$, $B_q = 0.25$, $M_1 = 4$ with $\mathcal{N}_* = 60$, $g = 1.0$, $f = 1.0 \times 10^{-2}$ are summarized in Table. 2.

d	Constraints on N	Constraints on N_1
2	$3.6 \times 10^7 \leq N \leq 4.5 \times 10^8$	$66 \leq N_1 \leq 76$
3	$4.5 \times 10^3 \leq N \leq 1.6 \times 10^4$	$37 \leq N_1 \leq 42$
4	$2.4 \times 10^2 \leq N \leq 5.6 \times 10^2$	$26 \leq N_1 \leq 28$
5	$57 \leq N \leq 1.1 \times 10^2$	$20 \leq N_1 \leq 22$
6	$24 \leq N \leq 41$	$17 \leq N_1 \leq 18$

Table 2: The constraints on N and N_1 derived from the lower and upper bound on F , (3.27) and (3.28), for the model $q = 3$, $B_q = 0.25$, $M_1 = 4$ with $\mathcal{N}_* = 60$, $g = 1.0$, $f = 1.0 \times 10^{-2}$.

We observe that for the cases $d \geq 5$, the condition (3.25) does not hold for the cases $d = 5$ and $d = 6$. In the case $d = 4$, the left hand side and the right hand side of the inequality in (3.25) are of the same order and we may better have a closer look. In Fig. 9, N/N_1 and F are plotted for the range of F of interest. We observe that two lines in the plot intersect at $F = 14$. However, notice that the inequality in (3.25) allows the both sides to be around the same. Therefore, we should not rule out the region $F > 14$ immediately. In fact, we observe from Fig. 9 that the both sides of (3.25) are around the same throughout the range of F of interest.

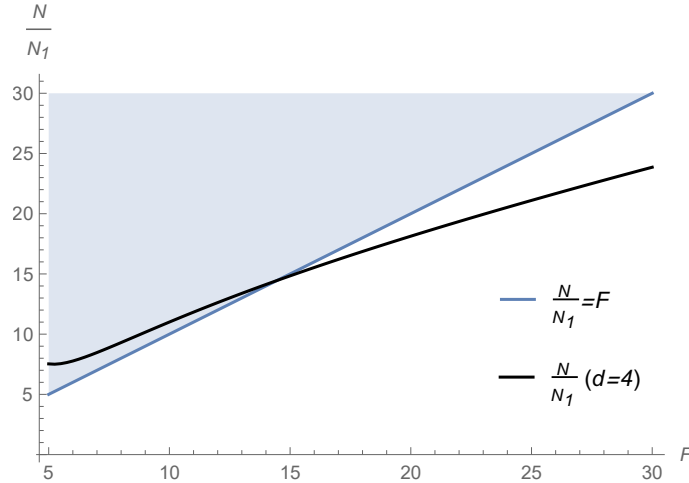


Figure 9: The plot of N/N_1 and the constraint on it that the model to be described as a single-field inflation model (3.25) for the range of F of interest.

We should also examine the constraint (3.26). We plot the numerically evaluated values of H_* for the range of F of interest in Fig. 10. We observe that H_* is of the order

of 10^{-5} . Putting $g \sim 1$ and $f \sim 10^{-2}$, (3.26) gives $N \ll 10^3$. Comparing this constraint with Table. 2, the cases $d \leq 3$ are excluded for these values of parameters g and f , while the $d \geq 5$ cases are safely in the allowed region. In the case $d = 4$, the allowed values of N in Table. 2 are comparable with the boundary of the constraint (3.26) in the range of F of interest, so we should have a closer look. In Fig. 11, we plotted N for the case $d = 4$ and the constraint from (3.26). We observe that the region $F > 15$ is excluded by the constraint (3.26) for the case $d = 4$, and as a consequence N is restricted as $N \leq 3.9 \times 10^2$ and N_1 is restricted as $N_1 \geq 26$.

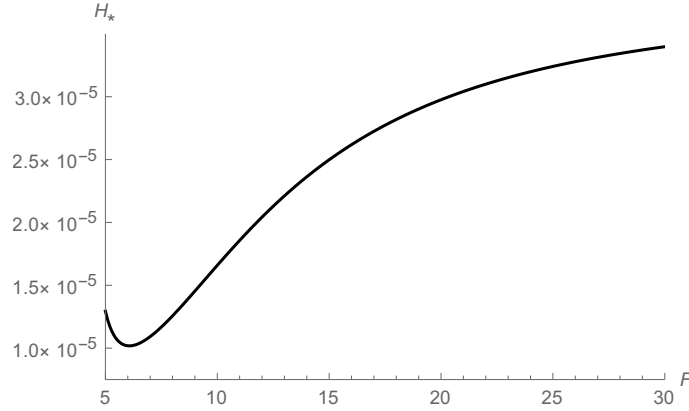


Figure 10: The plot of the Hubble parameter at the pivot scale for the model $q = 3$, $B_q = 0.25$, $M_1 = 4$ with $\mathcal{N}_* = 60$ for the range of F of interest $F_{l.b.} = 6.9 \leq F \leq F_{u.b.} = 26$.

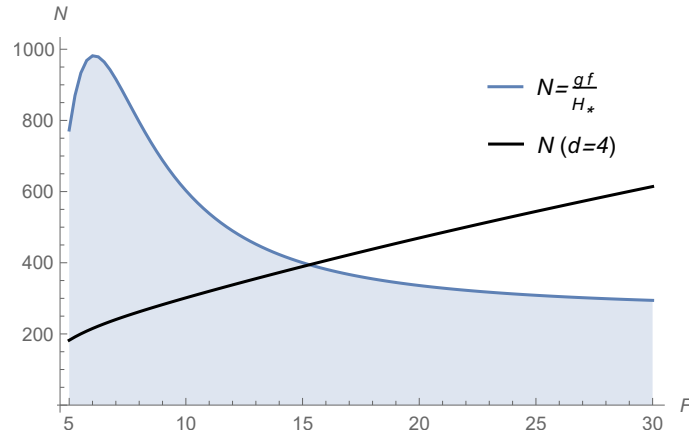


Figure 11: The constraint on N placed by (3.26) for the model $q = 3$, $B_q = 0.25$, $M_1 = 4$ with $\mathcal{N}_* = 60$ for the range of F of interest $F_{l.b.} = 6.9 \leq F \leq F_{u.b.} = 26$. The parameters g and f are fixed as $g = 1.0$ and $f = 1.0 \times 10^{-2}$ here. N for the case $d = 4$ in the same model with the same values of the parameters is plotted to be compared with the constraint.

To summarize the results of this model with parameter values $\mathcal{N}_* = 60$, $g = 1.0$ and $f = 1.0 \times 10^{-2}$, the cases $d \leq 3$ are excluded by the condition (3.26), while the cases $d \geq 5$, the condition (3.25) is not satisfied. In the case $d = 4$, we obtain $F \geq 6.9$ (which corresponds to $N \geq 2.4 \times 10^2$ and $N_1 \leq 28$) from the lower bound on n_s as in (3.27), and we obtain $F \leq 15$ (which corresponds to $N \leq 3.9 \times 10^2$ and $N_1 \geq 26$) from (3.26). Notice that in this range of the parameter F , the predicted tensor-to-scalar ratio r is above 0.01, as seen in Fig. 7. Like the previous model, this means via the Lyth bound [17] that the model is a large-field inflation model.

3.2 Particle production during inflation

The coupling of the inflaton and the charged matter fields in (2.22) is of the form investigated in [13, 12], which leads to rapid particle productions during inflation and may leave observable features in primordial density perturbation [18, 19, 20, 21, 22]. Below, we examine the detectability of the primordial features produced by the rapid particle productions during inflation.

The mass term of the charged matter with charge q is given as (2.26)

$$\tilde{\chi}_{(n_1)}^{q\dagger} M_{n_1}^2(q, \phi) \tilde{\chi}_{(n_1)}^q = \tilde{\chi}_{(n_1)}^{q\dagger} 4\gamma_1^q f^2 \sin^2 \left(\frac{q\phi + 2\pi n_1 F}{2FN_1} \right)^2 \tilde{\chi}_{(n_1)}^q, \quad (3.30)$$

where we have dropped m^2 term in (2.26), since only the fields with $m^2 \ll H^2$ will be relevant in the discussions below, whose effects can be well approximated by taking $m^2 = 0$. Near $\phi = -2\pi n_1 F/q$, the inflaton-dependent mass term of the matter field can be approximated as

$$\tilde{\chi}_{(n_1)}^{q\dagger} M_{n_1}^2(q, \phi) \tilde{\chi}_{(n_1)}^q \simeq \tilde{\chi}_{(n_1)}^{q\dagger} \frac{\gamma_1^q q^2}{N_1 N^{d-1}} \left(\phi + \frac{2\pi n_1 F}{q} \right)^2 \tilde{\chi}_{(n_1)}^q. \quad (3.31)$$

From the analytic result of [22], the contribution of the rapid particle production due to the interaction (3.31) to the power spectrum δP_s is given by

$$\delta := \frac{\delta P_s}{P_s} \simeq 2 \times 300 \left(\frac{qg}{N_1^{\frac{1}{2}} N^{\frac{d-1}{2}}} \right)^{7/2}, \quad (3.32)$$

where the factor 2 in the right hand side is from the fact that the complex field $\chi_{(n_I)}^q$ has two real degrees of freedom. We also restrict ourselves to the the universality restoration point $\gamma_I^q = g^2$ ($I = 1, \dots, d$), at which the KK mass spectra of the charged scalar fields coincide with that of the gauge field [12]. For the detectability of the primordial feature in the near future, we require that the amplitude of the feature to be more than a percent of the power spectrum:

$$\delta > 0.01. \quad (3.33)$$

Substituting (3.32) into (3.33) and the validity of the perturbation theory $gq \lesssim 1$, we obtain

$$N_1 N^{d-1} \lesssim 6 \times 10^2. \quad (3.34)$$

Using (2.18), (3.34) can be rewritten as

$$N_1^2 \lesssim 6 \times 10^2 \frac{f^2}{F^2}. \quad (3.35)$$

The EFT described by the action (2.1) is valid below $4\pi f$. It is natural to assume that this UV cut-off scale is still much below the Planck scale:

$$4\pi f \ll M_P. \quad (3.36)$$

On the other hand, if we restrict ourselves to the large field inflation, the period $2\pi F$ should be super-Planckian:

$$F \gtrsim M_P. \quad (3.37)$$

Putting (3.36) and (3.37) into (3.35), we obtain

$$N_1^2 \ll 4. \quad (3.38)$$

The condition (3.38) cannot be satisfied with an integer N_1 . Thus our (de)constructed model of extra-natural inflation does not produce detectable primordial feature under the rather general assumptions on the parameters, (3.36) and (3.37). Note that this conclusion is quite general: We did not explicitly specify q , B_q and M_1 in the above arguments. Their influence enters only through the observationally allowed range of F for these parameters, which generically satisfies (3.37).

4 Summary and discussions

In this article, we constructed (de)constructed models of extra-natural inflation which successfully explain the CMB observations. We overcome the obstacle for (de)constructing extra-natural inflation pointed out in [9] by introducing multiple (de)constructed extra dimensions, building on our previous work [12]. We compared the models with explicit choice of charged matter contents with CMB observations, and derived the constraints on the model parameters. The models were observationally viable in a region of the parameter space. We confirmed that the models successfully achieved the trans-Planckian inflaton field excursion. We also examined the mechanism of particle production during inflation which may leave features in primordial density perturbation [13, 12]. Under the natural and quite general assumptions, we showed that the primordial features from our (de)constructed extra-natural inflation models would not be detectable in cosmological observations.

The natural inflation model with a single sinusoidal potential is not favored by the latest CMB observations [16]. However, simple modifications of the single sinusoidal potential may improve the fit to the observational data. In this article, we studied multi-natural inflation proposed in [14] as such an improved model. Our (de)construction model provides a microscopic theory of multi-natural inflation. It will be interesting to explore other modifications of the inflaton potential from the simplest single sinusoidal potential which can arise from (de)construction.

It will also be interesting to explore (de)constructed extra-natural inflation models which predict detectable primordial features. Examining the quite general assumptions we have made to show that our models do not produce detectable primordial features may provide a starting point for finding such models.

In this article, we restrict ourselves to the regime where the number of the lattice points in each direction is large. In this regime, the resulting inflaton potential coincides with that from ordinary extra dimensions in the leading order, although the microscopic models do have different model parameters with their own range of applicability. In the meantime, the difference between the ordinary extra dimensions and the (de)constructed extra dimensions becomes sharper when the number of the lattice points in each direction is small. Thus it will be interesting to explore the regime in which the number of the lattice points in each direction is small.

Acknowledgments

This work is supported in part by the Science and Engineering Research Board, Department of Science and Technology, Government of India under the project file number EMR/2015/002471. The work of Suvedha Suresh Naik is supported by Dr. T.M.A. Pai PhD scholarship program of Manipal Academy of Higher Education. Manipal Centre for Natural Sciences, Centre of Excellence, Manipal Academy of Higher Education is acknowledged for facilities and support.

A Discrete Fourier Transform

We follow the same convention for the Discrete Fourier Transform (DFT) as used in [12]. It is reviewed here for the convenience of the readers.

Let us first consider the DFT in one-dimensional periodic lattice. Let us consider a cyclically ordered N points labeled by j ($j = 0, 1, \dots, N - 1 \pmod{N}$). Consider a variable ϕ_j which has a value on each point. We use the following convention for the

discrete Fourier expansion of the variable ϕ_j :

$$\phi_j = \frac{1}{\sqrt{N}} \sum_{n=-\frac{N-1}{2}}^{\frac{N-1}{2}} \tilde{\phi}_n e^{i\frac{2\pi nj}{N}} \quad (N : \text{odd}). \quad (\text{A.1})$$

$$\phi_j = \frac{1}{\sqrt{N}} \sum_{n=-\frac{N}{2}-1}^{\frac{N}{2}-1} \tilde{\phi}_n e^{i\frac{2\pi nj}{N}} + \frac{1}{\sqrt{N}} \tilde{\phi}_{\frac{N}{2}} (-)^j \quad (N : \text{even}). \quad (\text{A.2})$$

Our convention is convenient since when applied in (de)construction, each KK mode is canonically normalized.

When ϕ_j is a real variable, $\tilde{\phi}_{-n}^* = \tilde{f}_n$. The orthogonality of the exponential function:

$$\sum_{j=0}^{N-1} \left(e^{i\frac{2\pi n_1 j}{N}} \right)^* e^{i\frac{2\pi n_2 j}{N}} = N \delta_{n_1 n_2}, \quad (\text{A.3})$$

leads to the following formula for the discrete Fourier coefficient:

$$\tilde{\phi}_n = \frac{1}{\sqrt{N}} \sum_{j=0}^{N-1} \phi_j e^{-i\frac{2\pi nj}{N}}. \quad (\text{A.4})$$

The generalization of the DFT to d -dimensional periodic lattice is straightforward: One just need to repeat the same procedure as above for each direction. Let N_I be the number of the points in I -th direction ($I = 1, 2, \dots, d$). The discrete Fourier expansion is given as

$$\phi_{(\vec{j})} = \frac{1}{\prod_{I=1}^d N_I^{1/2}} \sum_{n_1} \sum_{n_2} \cdots \sum_{n_d} \tilde{\phi}_{(\vec{n})} e^{i \sum_{J=1}^d \frac{2\pi n_J j_J}{N_J}}. \quad (\text{A.5})$$

Here, \vec{j} is a vector whose I -th component is j_I ($I = 1, 2, \dots, d$), and \vec{n} is a vector whose I -th component is n_I ($I = 1, 2, \dots, d$). Each sum over n_I ($I = 1, 2, \dots, d$) follows the convention (A.1) or (A.2).

The Fourier coefficients are given as

$$\tilde{\phi}_{(\vec{n})} = \frac{1}{\prod_{I=1}^d N_I^{1/2}} \sum_{j_1} \sum_{j_2} \cdots \sum_{j_d} \phi_{(\vec{j})} e^{-i \sum_{J=1}^d \frac{2\pi n_J j_J}{N_J}}. \quad (\text{A.6})$$

We call $\vec{n} = \vec{0}$ component of the Fourier coefficients “zero-mode.” Explicitly,

$$\tilde{\phi}_{(\vec{0})} = \frac{1}{\prod_{I=1}^d N_I^{1/2}} \sum_{j_1} \sum_{j_2} \cdots \sum_{j_d} \phi_{(\vec{j})}. \quad (\text{A.7})$$

When considering the discrete version of dimensional reduction, it is useful to know the value of $\phi_{(\vec{j})}$ when all the Fourier coefficients except the zero-mode are zero:

$$\phi_{(\vec{j})} \Big|_{\tilde{\phi}_{(\vec{n})}=0 \text{ except } \vec{n}=\vec{0}} = \frac{1}{\prod_{I=1}^d N_I^{1/2}} \tilde{\phi}_{(\vec{0})}. \quad (\text{A.8})$$

B One-loop effective potential

In this appendix, we derive the one-loop effective potential for the zero-mode. While in the case of $d = 1$, it is possible to write down the one-loop effective potential applicable for arbitrary number of the lattice points in a relatively simple form [8], we did not find such a simple expression for $d \geq 2$. Therefore, we will derive the one-loop effective potential in the leading order in the number of the lattice points following [15]. The result formally coincides with the case of continuum extra dimensions [6, 7].

Let us denote the contribution of a charged scalar with charge q and mass m to the one-loop effective potential for the zero-modes $\tilde{A}_{(\vec{0})}^I$:

$$V_{1\text{-loop}}^q(\tilde{A}_{(\vec{0})}^I) = \sum_{n_1} \sum_{n_2} \cdots \sum_{n_d} \int \frac{d^4 k}{(2\pi)^4} \ln \left[k^2 + m^2 + \sum_{I=1}^d M_{n_I}^2(q, \tilde{A}_{(\vec{0})}^I) \right], \quad (\text{B.1})$$

where

$$M_{n_I}^2(q, \tilde{A}_{(\vec{0})}^I) := \frac{2}{a_I^2} \left(1 - \cos \left[\frac{q \tilde{A}_{(\vec{0})}^I}{\mathcal{F}_I} + \frac{2\pi n_I}{N_I} \right] \right), \quad (\text{B.2})$$

and

$$\mathcal{F}_I := f_I \prod_{J=1}^d N_J^{1/2}. \quad (\text{B.3})$$

In the above, we have analytically continued to the Euclidean time. In (B.2), for simplicity, we restrict ourselves to the universality restoration point $\gamma_I = g^2$ ($I = 1, \dots, d$), at which the KK mass spectra of the charged scalar fields coincide with that of the gauge field [12].

It is convenient to define

$$\zeta_q(s) := \sum_{n_1} \sum_{n_2} \cdots \sum_{n_d} \int \frac{d^4 k}{(2\pi)^4} \left[k^2 + m^2 + \sum_{I=1}^d M_{n_I}^2(q, \tilde{A}_{(\vec{0})}^I) \right]^{-s}. \quad (\text{B.4})$$

Using (B.4), the one-loop effective potential (B.1) can be written as

$$V_{1\text{-loop}}^q(\tilde{A}_{(\vec{0})}^I) = - \left. \frac{d\zeta_q(s)}{ds} \right|_{s=0}. \quad (\text{B.5})$$

We re-write (B.4) using the Schwinger parametrization:

$$\begin{aligned} \zeta_q(s) &= \sum_{n_1} \sum_{n_2} \cdots \sum_{n_d} \int \frac{d^4 k}{(2\pi)^4} \\ &\quad \frac{1}{\Gamma(s)} \int_0^\infty d\tau \tau^{s-1} \exp \left[-\tau \left(k^2 + m^2 + \sum_{I=1}^d M_{n_I}^2(q, \tilde{A}_{(\vec{0})}^I) \right) \right]. \end{aligned} \quad (\text{B.6})$$

After performing the Gaussian integral of k , we obtain

$$\zeta_q(s) = \sum_{n_1} \sum_{n_2} \cdots \sum_{n_d} \frac{1}{2(4\pi)^2} \frac{1}{\Gamma(s)} \int_0^\infty d\tau \tau^{s-3} \exp \left[-\tau \left(m^2 + \sum_{I=1}^d M_{n_I}^2(q, \tilde{A}_{(\vec{0})}^I) \right) \right]. \quad (\text{B.7})$$

Then, its derivative with respect to s gives

$$\left. \frac{d\zeta_q(s)}{ds} \right|_{s=0} = \sum_{n_1} \sum_{n_2} \cdots \sum_{n_d} \frac{1}{2(4\pi)^2} \int_0^\infty d\tau \tau^{s-3} \exp \left[-\tau \left(m^2 + \sum_{I=1}^d M_{n_I}^2(q, \tilde{A}_{(\vec{0})}^I) \right) \right] \Big|_{s=0}. \quad (\text{B.8})$$

In the above, we have used $\Gamma(s) \simeq 1/s + (\text{finite})$ in the limit $s \rightarrow 0$, and took the leading order term in the equation anticipating the limit $s \rightarrow 0$.

Substituting (B.8) into (B.5) gives

$$\begin{aligned} & V_{1\text{-loop}}^q(\tilde{A}_{(\vec{0})}^I) \\ &= - \sum_{n_1} \sum_{n_2} \cdots \sum_{n_d} \frac{1}{2(4\pi)^2} \int_0^\infty d\tau \tau^{-3} \exp \left[-\tau \left(m^2 + \sum_{I=1}^d M_{n_I}^2(q, \tilde{A}_{(\vec{0})}^I) \right) \right] \\ &= - \sum_{n_1} \sum_{n_2} \cdots \sum_{n_d} \frac{1}{2(4\pi)^2} \int_0^\infty d\tau \tau^{-3} \exp \left[-\tau \left(m^2 + \sum_{I=1}^d \frac{2}{a_I^2} \right) + \tau \sum_{I=1}^d \frac{2}{a_I^2} \cos \left[\frac{q\tilde{A}_{(\vec{0})}^I}{\mathcal{F}_I} + \frac{2\pi n_I}{N_I} \right] \right]. \end{aligned} \quad (\text{B.9})$$

Using the following identity for the modified Bessel function $I_\nu(z)$ with integer ν :

$$e^{z \cos \theta} = I_0(z) + 2 \sum_{\nu=1}^\infty I_\nu(z) \cos \theta, \quad (\text{B.10})$$

we can rewrite (B.9) as

$$\begin{aligned} & V_{1\text{-loop}}^q(\tilde{A}_{(\vec{0})}^I) \\ &= - \sum_{n_1} \sum_{n_2} \cdots \sum_{n_d} \frac{1}{2(4\pi)^2} \int_0^\infty d\tau \tau^{-3} \exp \left[-\tau \left(m^2 + \sum_{I=1}^d \frac{2}{a_I^2} \right) + \tau \sum_{I=1}^d \frac{2}{a_I^2} \cos \left[\frac{q\tilde{A}_{(\vec{0})}^I}{\mathcal{F}_I} + \frac{2\pi n_I}{N_I} \right] \right] \\ &= - \sum_{\ell_1=0}^\infty \sum_{\ell_2=0}^\infty \cdots \sum_{\ell_d=0}^\infty \frac{1}{2(4\pi)^2} \int_0^\infty d\tau \tau^{-3} \exp \left[-\tau \left(m^2 + \sum_{I=1}^d \frac{2}{a_I^2} \right) \right] \\ & \quad \left\{ 2^d \prod_{I=1}^d N_I I_{N_I \ell_I} \left(\frac{2\tau}{a_I^2} \right) \cos \left[\frac{N_I \ell_I q \tilde{A}_{(\vec{0})}^I}{\mathcal{F}_I} \right] \right\}. \end{aligned} \quad (\text{B.11})$$

On the other hand, we can expand the one-loop effective potential in Fourier mode with respect to $\tilde{A}_{(\vec{0})}^I$ ($I = 1, 2, \dots, d$):

$$V_{1\text{-loop}}^q(\tilde{A}_{(\vec{0})}^I) = \sum_{\ell_1=0}^\infty \sum_{\ell_2=0}^\infty \cdots \sum_{\ell_d=0}^\infty V_{\vec{\ell}} \prod_{I=1}^d \cos \left[\frac{q \ell_I N_I \tilde{A}_{(\vec{0})}^I}{\mathcal{F}_I} \right]. \quad (\text{B.12})$$

Here, $\vec{\ell}$ is a vector whose I -th component is ℓ_I .

Let us first analyze the simpler case $m^2 = 0$. Using the integral representation of the modified Bessel function with integer ν following from (B.10):

$$I_\nu(z) = \frac{1}{\pi} \int_0^\pi d\theta e^{z \cos \theta} \cos(\nu\theta), \quad (\text{B.13})$$

and taking N_I large with $N_I a_I = 2\pi L_I$ fixed,⁵ we obtain

$$\begin{aligned}
& V_{\vec{\ell}} \\
&= -\frac{1}{2(4\pi)^2} \left(\frac{2}{\pi}\right)^d \int_0^\infty \frac{d\tau}{\tau^3} \prod_{I=1}^d \left\{ N_I \int_0^\pi d\theta_I \exp \left[-\frac{2N_I^2\tau}{(2\pi L_I)^2} (1 - \cos \theta_I) \right] \cos [N_I \ell_I \theta_I] \right\} \\
&= -\frac{1}{2 \cdot 2^d (4\pi)^2} \left(\frac{2}{\pi}\right)^d \int_0^\infty \frac{d\tau}{\tau^3} \prod_{I=1}^d \left\{ N_I \int_0^\pi d\theta_I \right. \\
&\quad \left(\exp \left[-\frac{\tau}{(2\pi L_I)^2} \left(N_I^2 \theta_I^2 + i \frac{(2\pi L_I)^2}{\tau} N_I \ell_I \theta_I \right) \right] \right. \\
&\quad \left. \left. + \exp \left[-\frac{\tau}{(2\pi L_I)^2} \left(N_I^2 \theta_I^2 - i \frac{(2\pi L_I)^2}{\tau} N_I \ell_I \theta_I \right) \right] \right) \right\} + \mathcal{O}(N_I^{-2}) \\
&= -\frac{1}{2 \cdot 2^d (4\pi)^2} \left(\frac{2}{\pi}\right)^d \int_0^\infty \frac{d\tau}{\tau^3} \prod_{I=1}^d \left\{ \int_0^{N_I\pi} d\tilde{\theta}_I \left(\exp \left[-\frac{\tau}{(2\pi L_I)^2} \left(\tilde{\theta}_I^2 + i \frac{(2\pi L_I)^2}{\tau} \ell_I \tilde{\theta}_I \right) \right] \right. \right. \\
&\quad \left. \left. + \exp \left[-\frac{\tau}{(2\pi L_I)^2} \left(\tilde{\theta}_I^2 - i \frac{(2\pi L_I)^2}{\tau} \ell_I \tilde{\theta}_I \right) \right] \right) \right\} + \mathcal{O}(N_I^{-2}) \quad (\tilde{\theta}_I = N_I \theta_I) \\
&= -\frac{1}{2(4\pi)^2} \left(\frac{2}{\pi}\right)^d \int_0^\infty \frac{d\tau}{\tau^3} \prod_{I=1}^d \left\{ \left(\frac{\pi(2\pi L_I)^2}{\tau} \right)^{1/2} \exp \left[-\frac{(2\pi L_I)^2 \ell_I^2}{4\tau} \right] \right\} \\
&\quad + \mathcal{O}(N_I^{-2}) + \mathcal{O} \left(N_I^{-1} e^{-(\pi N_I)^2} \right) \\
&= -\frac{1}{2(4\pi)^2} \frac{2^d}{\pi^{d/2}} \int_0^\infty d\tilde{\tau} \tilde{\tau}^{1+\frac{d}{2}} \prod_{I=1}^d \left\{ (2\pi L_I) \exp \left[-\frac{(2\pi L_I)^2 \ell_I^2 \tilde{\tau}}{4} \right] \right\} \\
&\quad + \mathcal{O}(N_I^{-2}) + \mathcal{O} \left(N_I^{-1} e^{-(\pi N_I)^2} \right) \quad \left(\tilde{\tau} = \frac{1}{\tau} \right) \\
&= -\frac{1}{2(4\pi)^2} \frac{2^d}{\pi^{d/2}} \prod_{I=1}^d (2\pi L_I) \left(\frac{4}{\sum_{I=1}^d (2\pi L_I)^2 \ell_I^2} \right)^{2+\frac{d}{2}} \int_0^\infty dt t^{1+\frac{d}{2}} e^{-t} \\
&\quad + \mathcal{O}(N_I^{-2}) + \mathcal{O} \left(N_I^{-1} e^{-(\pi N_I)^2} \right) \quad \left(\frac{\sum_{I=1}^d (2\pi L_I)^2 \ell_I^2}{4} \tilde{\tau} = t \right) \\
&= -\frac{1}{2(4\pi)^2} \frac{2^d}{\pi^{d/2}} \Gamma \left(2 + \frac{d}{2} \right) \prod_{I=1}^d (2\pi L_I) \left(\frac{4}{\sum_{I=1}^d (2\pi L_I)^2 \ell_I^2} \right)^{2+\frac{d}{2}} + \mathcal{O}(N_I^{-2}) + \mathcal{O} \left(N_I^{-1} e^{-(\pi N_I)^2} \right).
\end{aligned} \tag{B.14}$$

⁵When $N_I \geq 3$, the limit $s \rightarrow 0$ does not lead to a divergence other than the constant term, which we fine-tune [8]. This result has already been used in (B.9).

In the above, we have used

$$\operatorname{erfc} x := \frac{2}{\sqrt{\pi}} \int_x^\infty dt e^{-t^2} = \frac{e^{-x^2}}{x\sqrt{\pi}} \sum_{n=0}^{\infty} \frac{(-)^n (2n-1)!!}{(2x^2)^n}. \quad (\text{B.15})$$

Next we turn to the case $m^2 \neq 0$.

$$\begin{aligned}
& V_{\vec{\ell}} \\
&= -\frac{1}{2(4\pi)^2} \left(\frac{2}{\pi}\right)^d \int_0^\infty \frac{d\tau}{\tau^3} e^{-\tau m^2} \prod_{I=1}^d \left\{ N_I \int_0^\pi d\theta_I \exp \left[-\frac{2N_I^2 \tau}{(2\pi L_I)^2} (1 - \cos \theta_I) \right] \cos [N_I \ell_I \theta_I] \right\} \\
&= -\frac{1}{2 \cdot 2^d (4\pi)^2} \left(\frac{2}{\pi}\right)^d \int_0^\infty \frac{d\tau}{\tau^3} e^{-\tau m^2} \prod_{I=1}^d \left\{ N_I \int_0^\pi d\theta_I \right. \\
&\quad \left(\exp \left[-\frac{\tau}{(2\pi L_I)^2} \left(N_I^2 \theta_I^2 + i \frac{(2\pi L_I)^2}{\tau} N_I \ell_I \theta_I \right) \right] \right. \\
&\quad \left. \left. + \exp \left[-\frac{\tau}{(2\pi L_I)^2} \left(N_I^2 \theta_I^2 - i \frac{(2\pi L_I)^2}{\tau} N_I \ell_I \theta_I \right) \right] \right) \right\} + \mathcal{O}(N_I^{-2}) \\
&= -\frac{1}{2 \cdot 2^d (4\pi)^2} \left(\frac{2}{\pi}\right)^d \int_0^\infty \frac{d\tau}{\tau^3} e^{-\tau m^2} \prod_{I=1}^d \left\{ \int_0^{N_I \pi} d\tilde{\theta}_I \left(\exp \left[-\frac{\tau}{(2\pi L_I)^2} \left(\tilde{\theta}_I^2 + i \frac{(2\pi L_I)^2}{\tau} \ell_I \tilde{\theta}_I \right) \right] \right. \right. \\
&\quad \left. \left. + \exp \left[-\frac{\tau}{(2\pi L_I)^2} \left(\tilde{\theta}_I^2 - i \frac{(2\pi L_I)^2}{\tau} \ell_I \tilde{\theta}_I \right) \right] \right) \right\} + \mathcal{O}(N_I^{-2}) \quad (\tilde{\theta}_I = N_I \theta_I) \\
&= -\frac{1}{2(4\pi)^2} \left(\frac{2}{\pi}\right)^d \int_0^\infty \frac{d\tau}{\tau^3} e^{-\tau m^2} \prod_{I=1}^d \left\{ \left(\frac{\pi (2\pi L_I)^2}{\tau} \right)^{1/2} \exp \left[-\frac{(2\pi L_I)^2 \ell_I^2}{4\tau} \right] \right\} \\
&\quad + \mathcal{O}(N_I^{-2}) + \mathcal{O} \left(N_I^{-1} e^{-(\pi N_I)^2} \right) \\
&= -\frac{1}{2(4\pi)^2} \frac{2^d}{\pi^{d/2}} \int_0^\infty d\tilde{\tau} e^{-\frac{m^2}{\tilde{\tau}}} \tilde{\tau}^{1+\frac{d}{2}} \prod_{I=1}^d \left\{ (2\pi L_I) \exp \left[-\frac{(2\pi L_I)^2 \ell_I^2 \tilde{\tau}}{4} \right] \right\} \\
&\quad + \mathcal{O}(N_I^{-2}) + \mathcal{O} \left(N_I^{-1} e^{-(\pi N_I)^2} \right) \quad \left(\tilde{\tau} = \frac{1}{\tau} \right) \\
&= -\frac{1}{2(4\pi)^2} \frac{2^d}{\pi^{d/2}} \prod_{I=1}^d (2\pi L_I) \left(\frac{4}{\sum_{I=1}^d (2\pi L_I)^2 \ell_I^2} \right)^{2+\frac{d}{2}} \int_0^\infty dt t^{1+\frac{d}{2}} e^{-t - \frac{z^2}{4t}} \\
&\quad + \mathcal{O}(N_I^{-2}) + \mathcal{O} \left(N_I^{-1} e^{-(\pi N_I)^2} \right) \quad \left(\frac{\sum_{I=1}^d (2\pi L_I)^2 \ell_I^2}{4} \tilde{\tau} = t, \quad z^2 = m^2 \sum_{I=1}^d (2\pi L_I)^2 \ell_I^2 \right) \\
&= -\frac{1}{2(4\pi)^2} \frac{2^d}{\pi^{d/2}} 2 \left(\frac{z}{2}\right)^{-2-\frac{d}{2}} K_{-(2+\frac{d}{2})}(z) \prod_{I=1}^d (2\pi L_I) \left(\frac{4}{\sum_{J=1}^d (2\pi L_J)^2 \ell_J^2} \right)^{2+\frac{d}{2}} \\
&\quad + \mathcal{O}(N_I^{-2}) + \mathcal{O} \left(N_I^{-1} e^{-(\pi N_I)^2} \right). \tag{B.16}
\end{aligned}$$

In the above, we have used the integral representation of the modified Bessel function

$$\int_0^\infty dt e^{-t - \frac{z^2}{4t}} t^{\nu-1} = 2 \left(\frac{z}{2}\right)^\nu K_{-\nu}(z), \tag{B.17}$$

which is valid for $|\arg z| < \frac{\pi}{4}$.

Using the limit $z \rightarrow 0$,

$$\int_0^\infty dt e^{-t - \frac{z^2}{4t}} t^{\nu-1} \rightarrow \Gamma(\nu) + \mathcal{O}(z^2), \quad (\text{B.18})$$

we recover the previous result (B.14) for the case $m^2 = 0$. In the meantime, from the asymptotic expansion of $K_\nu(z)$ for large z :

$$K_\nu(z) \sim \sqrt{\frac{\pi}{2z}} e^{-z} \sum_{n=0}^{\infty} \frac{(\nu, n)}{(2z)^n}, \quad (\text{B.19})$$

where

$$\begin{aligned} (\nu, n) &= \frac{\Gamma(\nu + n + \frac{1}{2})}{n! \Gamma(\nu - n + \frac{1}{2})} \quad (n \neq 0), \\ (\nu, 0) &= 1, \end{aligned} \quad (\text{B.20})$$

we observe that when $m^2 \gg 1/L_I^2$, the contribution to the one-loop effective potential is exponentially suppressed. Therefore, when calculating the one-loop effective potential, we can safely neglect the contributions from the fields which have mass above the KK-scale. In the meantime, the contribution of the fields which are much lighter than the KK-scale can be approximated by the massless limit using (B.18).

In this article, we set

$$f_I = f \quad (\text{for all } I), \quad (\text{B.21})$$

$$N_I = N \quad (\text{for all } I \neq 1), \quad (\text{B.22})$$

$$N \gg N_1. \quad (\text{B.23})$$

From (B.21), (B.22) and (2.8), all L_I except $I = 1$ are the same. We denote $L_I = L$ for all $I \neq 1$. As described in the main body, with the simplifying assumptions (B.21) and (B.22), the condition (B.23) can be used to make the potential such that in the $\phi := \tilde{A}_{(\vec{0})}^1$ direction satisfies the slow-roll condition while the $\tilde{A}_{(\vec{0})}^I$ directions ($I \neq 1$) do not. Then, during inflation we can safely set $\tilde{A}_{(\vec{0})}^I$ ($I \neq 1$) to its value at the bottom of the potential: $\tilde{A}_{(\vec{0})}^I = 0$ for $I \neq 1$, and the model is described as a single-field inflation model.

We approximate the one-loop effective potential of ϕ by taking only $\vec{\ell} = (1, 0, \dots, 0)$ term in (B.12), since the remaining terms rapidly decrease with ℓ_I .⁶ We obtain

$$V_{1\text{-loop}}^q(\tilde{A}_{(\vec{0})}^1 = \phi, \tilde{A}_{(\vec{0})}^I = 0 (I \neq 1)) \simeq V^q(\phi) := -\Lambda^4 \cos \left[\frac{q\phi}{F} \right], \quad (\text{B.24})$$

⁶The terms omitted here might have relevance in future observations, for example, in the observations of the running of the spectral index or the further running of it [23].

where

$$\begin{aligned}\Lambda^4 &= \frac{1}{2(4\pi)^2} \frac{2^d}{\pi^{d/2}} \Gamma\left(2 + \frac{d}{2}\right) (2\pi L_1)(2\pi L)^{d-1} \left(\frac{4}{(2\pi L_1)^2}\right)^{2+\frac{d}{2}} \\ &= \frac{1}{2(4\pi)^2} \frac{2^d}{\pi^{d/2}} \Gamma\left(2 + \frac{d}{2}\right) N_1 N^{d-1} \left(\frac{2}{N_1}\right)^{4+d} (gf)^4,\end{aligned}\tag{B.25}$$

and

$$F = \frac{N^{\frac{d-1}{2}} f}{N_1^{\frac{1}{2}}}.\tag{B.26}$$

C Fitting Functions

As explained in the main body, for generic values of parameters, we cannot analytically perform integration in (3.11) to have explicit functional form of \mathcal{N}_* as a function of ϕ_* , or ϕ_* as a function of \mathcal{N}_* . As a result, we do not have an explicit functional form $\Phi[F]$ given in (3.20) or (3.29). This makes it hard to understand the dependence of the model predictions on the parameter F without relying on numerical tools. To ease this issue, it is convenient to have a fitting function $\Phi_{fit}[F]$ which approximates $\Phi[F]$ for the range of F of interest. For this purpose, we first numerically evaluate the values of $\Phi[F]$ for the range of F of interest with step 0.1. Then we fit the logarithm of these values with a polynomial with degree two. The exponential of this fitting polynomial can be used as an approximation to $\Phi[F]$.

Similarly, when q , B_q and \mathcal{N}_* are fixed, $H_* := H(\phi_*)$ in (3.14) depends only on the parameter F . We numerically evaluate values of H_*^2 for the range of F of interest with step 0.1, and fit these values with a polynomial of degree two.

The model $q = 2$, $B_q = 0.2$, $M_1 = 5$ with $\mathcal{N}_* = 60$

The fitting function for $\Phi[F]$ we provide is

$$\Phi_{fit}[F] = \begin{cases} \exp[6.37 - 1.13F + 0.0526F^2] & (6.0 \leq F < 8.5), \\ \exp[3.44 - 0.425F + 0.00995F^2] & (8.5 \leq F \leq 16). \end{cases}\tag{C.1}$$

$\Phi[F]$ and $\Phi_{fit}[F]$ are plotted for the range of F of interest in Fig. 12. The error of the fit is plotted in Fig. 13. We observe that the size of the error is around 1% or less in the range of F of interest.

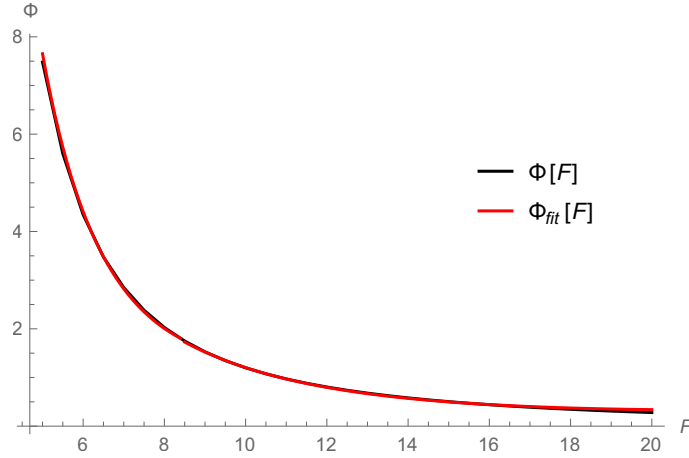


Figure 12: $\Phi[F]$ in (3.20) which is numerically evaluated (black) and the fitting polynomial $\Phi_{fit}[F]$ (red) are plotted for a range of values of F for the model $q = 2$, $B_q = 0.2$ with $\mathcal{N}_* = 60$.

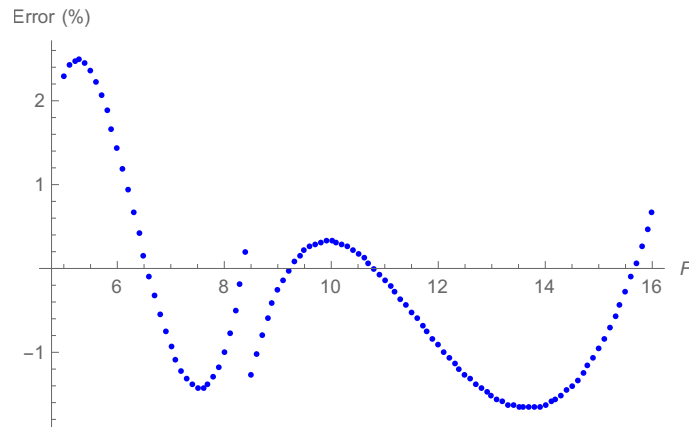


Figure 13: The plot of the error of the fitting $(\Phi_{fit}[F] - \Phi[F])/\Phi[F]$ in percent (%) for the model $q = 2$, $B_q = 0.2$ with $\mathcal{N}_* = 60$.

The fitting function we provide for H_*^2 is

$$H_{*fit}^2[F] = -6.02 \times 10^{-10} + 1.77 \times 10^{-10}F - 0.0116F^2. \quad (\text{C.2})$$

H_*^2 and H_{fit}^2 are plotted in Fig. 14. The error of the fit is plotted in Fig. 15. We observe that the size of the error is around 1% or less in the range of F of interest.

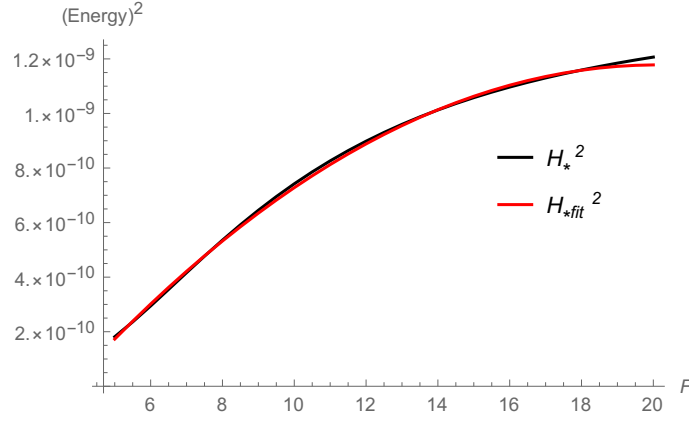


Figure 14: The plot of the square of the Hubble parameter at the pivot scale H_*^2 numerically evaluated (black) for the model $q = 2$, $B_q = 0.2$, $M_1 = 5$ with $\mathcal{N}_* = 60$ and the fitting polynomial $H_{*fit}^2[F]$ (C.2) (red) for the range of F of interest $F_{l.b.} = 6.4 \leq F \leq F_{u.b.} = 16$.

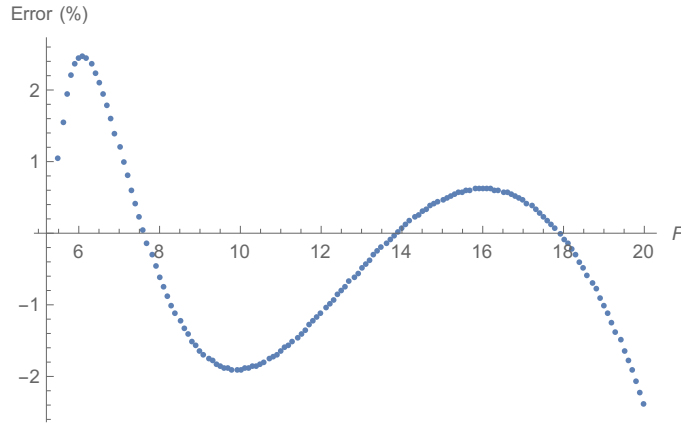


Figure 15: The plot of the error $(H_{*fit}^2 - H_*^2)/H_*^2$ in percent (%) for the model $q = 2$, $B_q = 0.2$, $M_1 = 5$ with $\mathcal{N}_* = 60$ for the range of F of interest $F_{l.b.} = 6.4 \leq F \leq F_{u.b.} = 16$.

The model $q = 3$, $B_q = 0.25$, $M_1 = 4$ with $\mathcal{N}_* = 60$

The fitting function for $\Phi[F]$ we provide is

$$\Phi_{fit}[F] = \begin{cases} \exp[4.99 - 0.508F + 0.0117F^2] & (7 \leq F < 15), \\ \exp[2.99 - 0.251F + 0.00346F^2] & (15 \leq F \leq 27). \end{cases} \quad (\text{C.3})$$

$\Phi[F]$ and $\Phi_{fit}[F]$ are plotted for the range of F of interest in Fig. 16. The error of the fit is plotted in Fig. 17. We observe that the size of the error is around 2% or less in the range of F of interest.

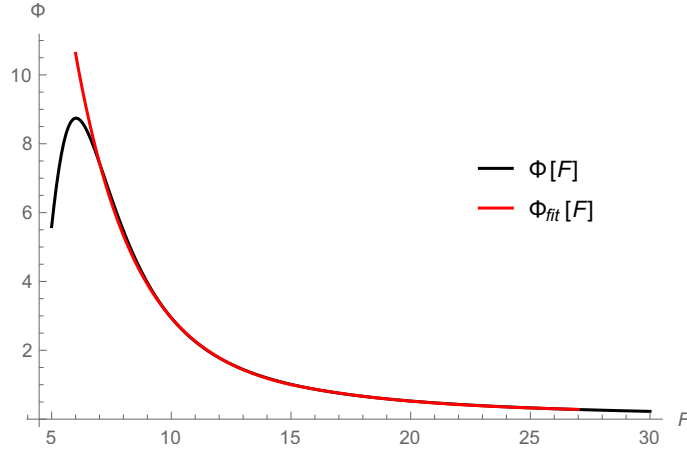


Figure 16: $\Phi[F]$ in (3.29) which is numerically evaluated (black) and the fitting polynomial $\Phi_{fit}[F]$ (red) are plotted for a range of values of F for the model $q = 3$, $B_q = 0.25$ with $\mathcal{N}_* = 60$.

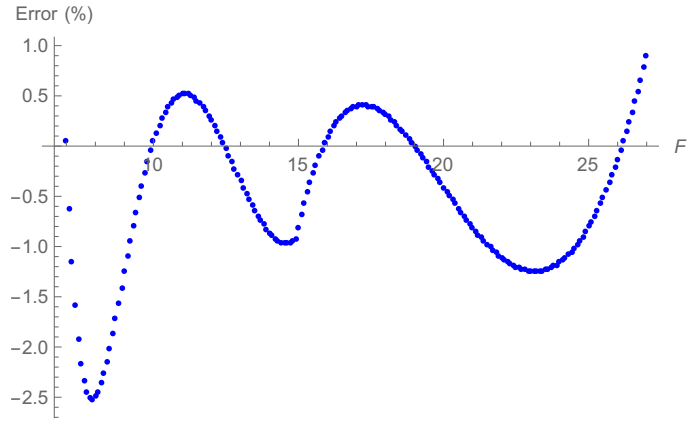


Figure 17: The plot of the error $(\Phi_{fit}[F] - \Phi[F])/\Phi[F]$ in percent (%) for the model $q = 3$, $B_q = 0.25$ with $\mathcal{N}_* = 60$.

The fitting function we provide for H_*^2 is

$$H_{*fit}^2[F] = \begin{cases} 5.04^{-11} - 1.97 \times 10^{-11}F + 4.19 \times 10^{-12}F^2 & (7 \leq F \leq 12), \\ -7.44^{-10} - 1.2 \times 10^{-10}F - 1.93 \times 10^{-12}F^2 & (12 < F \leq 27). \end{cases} \quad (\text{C.4})$$

H_*^2 and H_{*fit}^2 are plotted in Fig. 18. The error of the fit is plotted in Fig. 19. We observe that the size of the error is around 2% or less in the range of F of interest.

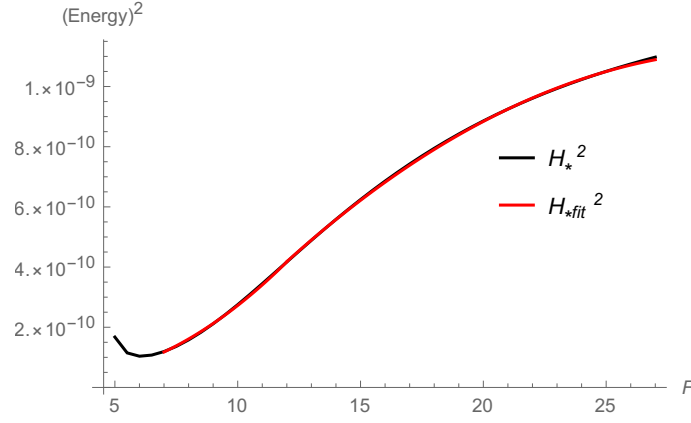


Figure 18: The plot of the square of the Hubble parameter at the pivot scale H_*^2 numerically evaluated (black) for the model $q = 3$, $B_q = 0.25$, $M_1 = 4$ with $\mathcal{N}_* = 60$ and the fitting polynomial H_{*fit}^2 (C.4) (red) for the range of F of interest $F_{l.b.} = 6.9 \leq F \leq F_{u.b.} = 26$.

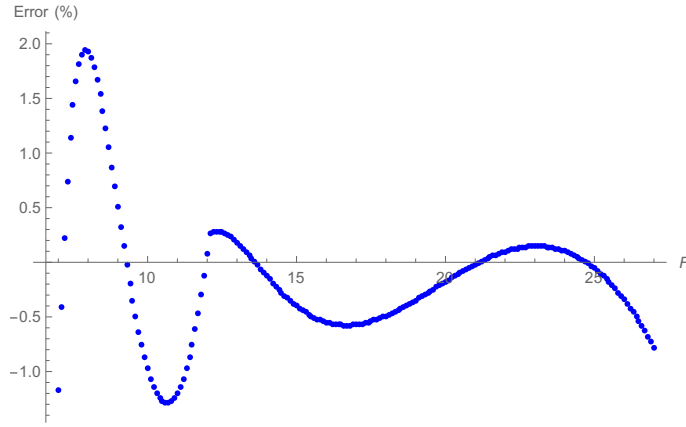


Figure 19: The plot of the error $(H_{*fit}^2 - H_*^2)/H_*^2$ in percent (%) for the model $q = 3$, $B_q = 0.25$, $M_1 = 4$ with $\mathcal{N}_* = 60$ for the range of F of interest $F_{l.b.} = 6.9 \leq F \leq F_{u.b.} = 26$.

References

- [1] N. Arkani-Hamed, A. G. Cohen, and H. Georgi, “(De)constructing dimensions,” *Phys. Rev. Lett.* **86** (2001) 4757–4761, [arXiv:hep-th/0104005](#) [hep-th].
- [2] C. T. Hill, S. Pokorski, and J. Wang, “Gauge Invariant Effective Lagrangian for Kaluza-Klein Modes,” *Phys. Rev.* **D64** (2001) 105005, [arXiv:hep-th/0104035](#) [hep-th].
- [3] Y. Hosotani, “Dynamical Mass Generation by Compact Extra Dimensions,” *Phys. Lett.* **126B** (1983) 309–313.
- [4] Y. Hosotani, “Dynamics of Nonintegrable Phases and Gauge Symmetry Breaking,” *Annals Phys.* **190** (1989) 233.
- [5] A. T. Davies and A. McLachlan, “Congruency Class Effects in the Hosotani Model,” *Nucl. Phys.* **B317** (1989) 237.
- [6] I. Antoniadis, “A Possible new dimension at a few TeV,” *Phys. Lett. B* **246** (1990) 377–384.
- [7] H. Hatanaka, T. Inami, and C. S. Lim, “The Gauge hierarchy problem and higher dimensional gauge theories,” *Mod. Phys. Lett.* **A13** (1998) 2601–2612, [arXiv:hep-th/9805067](#) [hep-th].
- [8] N. Arkani-Hamed, A. G. Cohen, and H. Georgi, “Electroweak symmetry breaking from dimensional deconstruction,” *Phys. Lett.* **B513** (2001) 232–240, [arXiv:hep-ph/0105239](#) [hep-ph].
- [9] N. Arkani-Hamed, H.-C. Cheng, P. Creminelli, and L. Randall, “Extra natural inflation,” *Phys. Rev. Lett.* **90** (2003) 221302, [arXiv:hep-th/0301218](#) [hep-th].
- [10] D. E. Kaplan and N. J. Weiner, “Little inflatons and gauge inflation,” *JCAP* **0402** (2004) 005, [arXiv:hep-ph/0302014](#) [hep-ph].
- [11] K. Freese, J. A. Frieman, and A. V. Olinto, “Natural inflation with pseudo - Nambu-Goldstone bosons,” *Phys.Rev.Lett.* **65** (1990) 3233–3236.
- [12] K. Furuuchi, S. S. Naik, and N. J. Jobu, “Large Field Excursions from Dimensional (De)construction,” [arXiv:2001.06518](#) [hep-th].
- [13] K. Furuuchi, “Excursions through KK modes,” *JCAP* **1607** no. 07, (2016) 008, [arXiv:1512.04684](#) [hep-th].

- [14] M. Czerny and F. Takahashi, “Multi-Natural Inflation,” *Phys. Lett.* **B733** (2014) 241–246, [arXiv:1401.5212 \[hep-ph\]](#).
- [15] K. Furuuchi, T. Inami, and K. Okuyama, “Gauge-Higgs Unification In Spontaneously Created Fuzzy Extra Dimensions,” *JHEP* **11** (2011) 006, [arXiv:1108.4462 \[hep-ph\]](#).
- [16] **Planck** Collaboration, Y. Akrami *et al.*, “Planck 2018 results. X. Constraints on inflation,” [arXiv:1807.06211 \[astro-ph.CO\]](#).
- [17] D. H. Lyth, “What would we learn by detecting a gravitational wave signal in the cosmic microwave background anisotropy?,” *Phys. Rev. Lett.* **78** (1997) 1861–1863, [arXiv:hep-ph/9606387](#).
- [18] L. Kofman, A. D. Linde, and A. A. Starobinsky, “Towards the theory of reheating after inflation,” *Phys. Rev.* **D56** (1997) 3258–3295, [arXiv:hep-ph/9704452 \[hep-ph\]](#).
- [19] D. J. H. Chung, E. W. Kolb, A. Riotto, and I. I. Tkachev, “Probing Planckian physics: Resonant production of particles during inflation and features in the primordial power spectrum,” *Phys. Rev.* **D62** (2000) 043508, [arXiv:hep-ph/9910437 \[hep-ph\]](#).
- [20] N. Barnaby, Z. Huang, L. Kofman, and D. Pogosyan, “Cosmological Fluctuations from Infra-Red Cascading During Inflation,” *Phys. Rev.* **D80** (2009) 043501, [arXiv:0902.0615 \[hep-th\]](#).
- [21] N. Barnaby and Z. Huang, “Particle Production During Inflation: Observational Constraints and Signatures,” *Phys. Rev.* **D80** (2009) 126018, [arXiv:0909.0751 \[astro-ph.CO\]](#).
- [22] L. Pearce, M. Peloso, and L. Sorbo, “Resonant particle production during inflation: a full analytical study,” *JCAP* **1705** no. 05, (2017) 054, [arXiv:1702.07661 \[astro-ph.CO\]](#).
- [23] K. Kohri, C. Lim, and C.-M. Lin, “Distinguishing between Extra Natural Inflation and Natural Inflation after BICEP2,” *JCAP* **08** (2014) 001, [arXiv:1405.0772 \[hep-ph\]](#).